

# AuthGlass: Benchmarking Voice Liveness Detection and Authentication on Smart Glasses via Comprehensive Acoustic Features

WEIYE XU, Tsinghua University, China  
 ZHANG JIANG, Tsinghua University, China  
 SIQI ZHENG, Tsinghua University, China  
 XIYUXING ZHANG, Tsinghua University, China  
 CHANGHAO ZHANG, Ant Group, China  
 JIAN LIU\*, Ant Group, China  
 WEIQIANG WANG, Ant Group, China  
 YUNTAO WANG\*, Tsinghua University, China

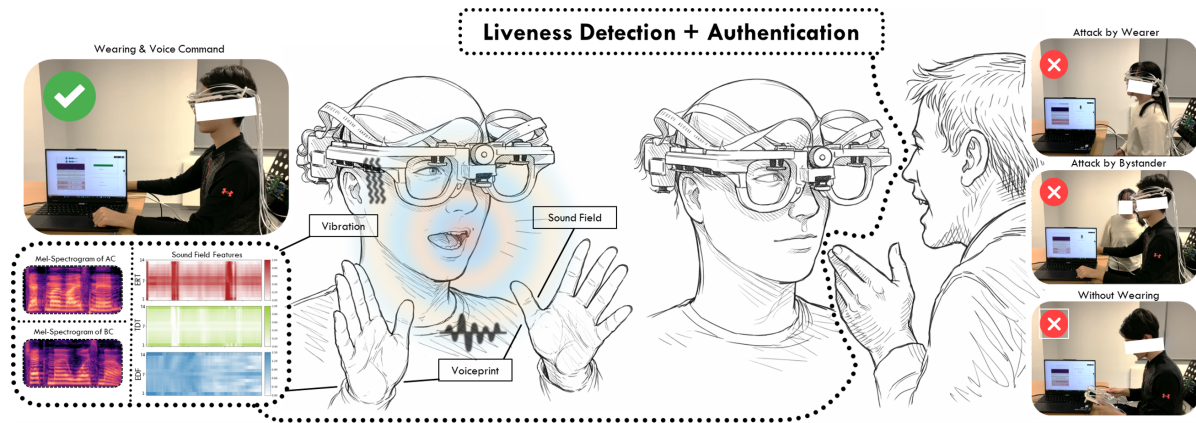


Fig. 1. Based on insights derived from our collected multi-acoustic sensing data, we develop AuthG-Live, which performs liveness detection using sound-field features, and AuthG-Net, which conducts authentication by jointly leveraging voiceprint, vibration, and sound-field features. The proposed framework is generalizable to different input-channel configurations. In this figure, liveness detection and authentication are demonstrated using five air-conductive microphones (consistent with Ray-Ban Meta [6]) mounted on the smart glasses and operating at a sampling rate of 16 kHz. As illustrated, the system successfully rejects three adversarial scenarios: attacks by the wearer, attacks by a bystander, and voice commands issued without wearing the device.

\*Co-corresponding authors.

Authors' Contact Information: Weiye Xu, Tsinghua University, Beijing, China, xuwy24@mails.tsinghua.edu.cn; Zhang Jiang, Tsinghua University, Beijing, China, jiangzhang20030102@gmail.com; Siqi Zheng, Tsinghua University, Beijing, China, ymzqwq@gmail.com; Xiyuxing Zhang, Tsinghua University, Beijing, China, zxyx22@mails.tsinghua.edu.cn; Changhao Zhang, Ant Group, Hangzhou, China, eleven.zch@antgroup.com; Jian Liu, Ant Group, Hangzhou, China, rex.lj@antgroup.com; Weiqiang Wang, Ant Group, Hangzhou, China, weiqiang.wwq@antgroup.com; Yuntao Wang, Tsinghua University, Beijing, China, yuntaowang@tsinghua.edu.cn.

Permission to make digital or hard copies of all or part of this work for personal or classroom use is granted without fee provided that copies are not made or distributed for profit or commercial advantage and that copies bear this notice and the full citation on the first page. Copyrights for components of this work owned by others than the author(s) must be honored. Abstracting with credit is permitted. To copy otherwise, or republish, to post on servers or to redistribute to lists, requires prior specific permission and/or a fee. Request permissions from permissions@acm.org.

With the rapid advancement of smart glasses, voice interaction has been widely adopted due to its naturalness and convenience. However, its practical deployment is often undermined by vulnerability to spoofing attacks, while no public dataset currently exists for voice liveness detection and authentication in smart-glasses scenarios. To address this challenge, we first collect a multi-acoustic-modal dataset comprising 16-channel audio data from 42 subjects, along with corresponding attack samples covering two attack categories. Based on insights derived from this collected data, we propose AuthG-Live, a sound-field-based voice liveness detection method, and AuthG-Net, a multi-acoustic-modal authentication model. We further benchmark seven voice liveness detection methods and four authentication methods across diverse acoustic modalities. The results demonstrate that our proposed approach achieves state-of-the-art performance on four benchmark tasks, and extensive ablation studies validate the generalizability of our methods across different modality combinations. Finally, we release this dataset, termed AuthGlass, to facilitate future research on voice liveness detection and authentication for smart glasses.

CCS Concepts: • **Do Not Use This Code** → **Generate the Correct Terms for Your Paper**; *Generate the Correct Terms for Your Paper*; Generate the Correct Terms for Your Paper; Generate the Correct Terms for Your Paper.

Additional Key Words and Phrases: Do, Not, Use, This, Code, Put, the, Correct, Terms, for, Your, Paper

#### ACM Reference Format:

Weiyu Xu, Zhang Jiang, Siqi Zheng, Xiyuxing Zhang, Changhao Zhang, Jian Liu, Weiqiang Wang, and Yuntao Wang. 2018. AuthGlass: Benchmarking Voice Liveness Detection and Authentication on Smart Glasses via Comprehensive Acoustic Features. In *Proceedings of Make sure to enter the correct conference title from your rights confirmation email (Proc. ACM Interact. Mob. Wearable Ubiquitous Technol.)*. ACM, New York, NY, USA, 37 pages. <https://doi.org/XXXXXXXX.XXXXXXX>

## 1 Introduction

In recent years, smart glasses have rapidly advanced, with commercial products such as Microsoft HoloLens [4] and Ray-Ban Meta Glasses [6] being widely adopted by users. Among various interaction modalities, voice input has been the most extensively integrated into smart glasses [6, 7] due to its intuitiveness, hands-free nature, and lightweight hardware requirements. Smart glasses equipped with voice interfaces are particularly useful in scenarios where users' hands are occupied [59] and commands need to be executed, such as driving [18, 30] and cooking [15, 49], where voice interaction has been shown to be effective.

However, as smart glasses become increasingly integrated with users' personal data, secure input mechanisms are becoming ever more critical [56]. To address this issue, various authentication methods have been proposed, including password-based schemes [34], iris recognition [39, 46], and gaze-based features [25]. Nevertheless, voice authentication remains the most straightforward and natural solution, as it can be seamlessly integrated into existing voice interfaces [56], which are already widely incorporated into smart glasses.

Although voice authentication has been extensively studied on smart devices and other wearables [38, 73, 78, 84], achieving robust performance on smart glasses remains challenging. The primary limitation lies in the lack of voice data collected directly from smart glasses, whose physical form factor differs significantly from other devices. While numerous solutions have been proposed for smartphones and other wearable devices such as earables [14, 24, 28, 42, 51, 84], it remains unclear whether these methods can be effectively generalized to smart glasses.

To address these challenges, we first developed a DIY smart glasses platform capable of capturing 16-channel synchronized, multi-acoustic-modal audio at a high sampling rate of 96 kHz. Based on this platform, we collected comprehensive utterance data from 42 users, along with attack samples under two attack types, forming the *AuthGlass* dataset. Leveraging this dataset, we gained insights into the acoustic characteristics captured by smart glasses and accordingly proposed a liveness detection method, *AuthG-Live*, based on sound-field features, as

---

*Proc. ACM Interact. Mob. Wearable Ubiquitous Technol.*, Woodstock, NY

© 2018 Copyright held by the owner/author(s). Publication rights licensed to ACM.

ACM ISBN 978-1-4503-XXXX-X/2018/06

<https://doi.org/XXXXXXXX.XXXXXXX>

well as a multi-acoustic-modal authentication model, *AuthG-Net*. Furthermore, we benchmarked seven liveness detection methods and four authentication methods covering different acoustic modalities, and validated that our approach achieves state-of-the-art performance across four benchmark tasks.

Specifically, our proposed method achieves a best liveness detection accuracy exceeding 96% and an authentication accuracy exceeding 97%. It also demonstrates strong generalizability across different attack types and supports cross-utterance authentication performance.

Through extensive ablation studies, we further validate that our liveness detection and authentication methods can be generalized to different acoustic channel configurations with acceptable performance. These results also provide useful design insights into microphone placement for smart glasses. To facilitate future research, we open-source both the dataset and the smart glasses platform implementation<sup>1</sup>.

Our key contributions are summarized as follows:

- We propose and open-source the AuthGlass dataset, which contains high-sampling-rate, 16-channel synchronized multi-acoustic-modal recordings from 42 participants, along with two attack scenarios. We also release the corresponding data capture platform.
- We propose AuthG-Live, a voice liveness detection method using sound-field features that generalizes across different attacks, and AuthG-Net, a multi-acoustic-modal voice authentication model supporting utterance-independent authentication.
- We benchmark seven voice liveness detection methods and four voice authentication methods across four tasks, demonstrating that our approach achieves state-of-the-art performance.
- Through ablation studies, we show that our methods remain effective under limited acoustic channel settings, including configurations consistent with real-world commercial products.

## 2 Related Works

This section summarizes the related works, including voice interface on smart glasses (Section 2.1), liveness detection and authentication on wearable devices (Section 2.2), and benchmark for liveness detection and authentication on smart glasses (Section 2.3)

### 2.1 Voice Interface on Smart Glasses

Voice user interfaces (VUIs) have long been explored as a natural and straightforward interaction modality, enabling intuitive human-computer interaction across a wide range of scenarios, such as smart home control [33, 65, 69], in-vehicle voice assistants [22, 35], and hands-free interaction for wearable devices [19]. For smart glasses, voice interfaces require only lightweight microphones for user interaction [54], making them particularly suitable for resource-constrained wearable devices. As a result, voice interaction has been widely adopted in commercial smart glasses, including Ray-Ban Meta [6], Xreal One Pro [9], and Rokid Glasses [7].

On the one hand, voice input is well suited for hands-free command execution and conversation-based AI functionalities, especially with the rapid growth of large language models. For example, Rokid has proposed voice-based payment functions, while Ray-Ban Meta leverages voice interaction to control AI-powered services and assistants.

On the other hand, prior research has explored the potential of voice-based interaction on smart glasses, particularly for assisting visually impaired users [26, 53, 60, 67]. Moreover, voice interfaces enable touchless interaction without diverting users' visual attention, making them especially suitable for emergency medical services [86] and industrial applications [40].

<sup>1</sup>We provide sample data and will release the full dataset and smart glasses prototype design files upon paper acceptance

As smart glasses increasingly integrate with users' personal information, securing their voice-based interfaces has become a critical challenge. However, with the rapid advancement of speech synthesis and deepfake technologies [37, 57, 70], voice interfaces are increasingly threatened by various types of attacks [23, 36, 82]. Since smart glasses are often exposed to surrounding speech and ambient noise, they are particularly vulnerable to forged or injected voice commands from adversaries [16, 44], potentially leading to severe privacy breaches. Prior studies [43, 77] have shown that authentication schemes relying solely on acoustic features remain vulnerable to diverse threats, including replay attacks [72, 82] and synthetic speech attacks [75, 88], thus lacking sufficient robustness.

Although several studies have enhanced voice input security through voice-related liveness detection and authentication on other wearables and smart devices [48, 74, 83], investigations targeting smart glasses remain limited. In particular, there is currently no dedicated hardware platform or comprehensive audio dataset tailored for smart glasses, resulting in the absence of standardized benchmarks for voice liveness detection and authentication in this domain. To address this gap, we implemented and open-sourced a DIY smart glasses prototype capable of comprehensive acoustic data capture across multiple acoustic modalities.

## 2.2 Liveness Detection and Authentication on Wearable Devices

Wearable devices such as earbuds and smart watches have been increasingly adopted in daily life, serving as personal computing and interaction platforms [61]. As these devices can collect and store sensitive user data and executing commands, ensuring secure access has become a critical concern [12].

Existing approaches for securing wearable devices can be categorized into two major directions: liveness detection and authentication. Liveness detection aims to distinguish genuine human from potential attack, while authentication focuses on verifying the claimed identity of the user. A variety of liveness detection and authentication techniques have been proposed for wearable platforms, leveraging different sensing modalities, including audio [11, 21, 31], motion [17, 66, 80], and physiological signals like PPG [87] and EMG [63]. In particular, voice-based solutions [11, 28, 64] have attracted significant attention due to their natural interaction paradigm and hands-free usability. For example, Huang et al. [32] leverage similarity of air-conductive and bone-conductive sound captured by microphones mounted on earbuds for liveness detection. While Gao et al. [28] leverages acoustic features extracted from in-ear and out-ear audio for user authentication.

Compared to other wearable devices, smart glasses exhibit unique characteristics in terms of voice-based sensing capabilities. Existing smart glasses [6, 7, 9] typically employ multiple microphones distributed around the eyeglass frame, resulting in inherently multi-channel audio inputs that capture rich spatial and acoustic information that can potentially be used for liveness detection and authentication [78, 81].

However, whether solutions for wearables could be generalized to smart glasses remains uncertain, and there is currently no unified hardware platform or publicly available dataset that enables systematic benchmarking of voice liveness detection and authentication methods on smart glasses. To address this gap, we collect multi-channel audio data using a multi-microphone DIY glasses platform. We also propose a multi-acoustic-modality-based liveness detection and authentication method, and benchmark representative passive acoustic methods using our dataset.

## 2.3 Benchmark for Liveness Detection and Authentication on Smart Glasses

Recent smart glasses increasingly adopt multi-channel audio as a primary input modality for voice interaction [6, 7, 9], which makes reliable voice liveness detection and authentication particularly critical for security-sensitive applications. Although voice liveness detection and speaker authentication have been extensively studied for conventional automatic speaker verification (ASV) systems, most existing datasets are not specifically designed for smart-glasses-based scenarios.

Table 1. Comparison of voice-based liveness detection or authentication systems on wearable devices.

Name	Hardware	Sampling Rate	Channels	Modalities	Open-Source
VOGUE[17]	Gyroscope embedded in existing device	44.1 kHz / 50 Hz	2	Air-conducted microphone + gyroscope	×
Vauth[24]	IMU manually mounted on glasses nose pad	44.1 kHz / 11 kHz	2	Air-conducted microphone + vibration sensor	×
Eve Said Yes[32]	BC microphone module manually mounted	48 kHz	2	Air-conducted microphone + bone-conducted microphone	×
Voshield[81]	Microphone array module	16 kHz	4	Air-conducted microphones	×
Ours	Multi-acoustic-modal microphone array on smart glasses frame	96 kHz	16	Multi air-conducted + bone-conducted microphones	✓

Several widely used public datasets, such as ASVspoof [76], VoxCeleb [52], RedDots Replayed [41], and SITW [50], provide rich audio recordings containing both genuine and spoofed samples, enabling the training and evaluation of liveness detection and authentication models for general voice assistant systems. However, these datasets are mainly collected using single-channel or limited microphone setups and do not reflect the physical form factor of smart glasses. In particular, they fail to capture the characteristics of multi-channel audio signals received by microphones distributed around the eyeglass frame, where spatial cues, channel-dependent energy distributions, and time-delay information are closely coupled with the wearable geometry.

On the other hand, several datasets have been collected using wearable or distributed microphone platforms to capture real-world multi-channel audio, such as REALMAN [79] and the Massive Distributed Microphone Array Dataset [20]. While these datasets provide realistic multi-channel recordings under wearable or spatially distributed configurations, they are not designed for ASV-related tasks and do not include replay or synthesis attacks. As a result, they cannot be directly used to evaluate voice liveness detection or authentication performance.

In parallel, a number of studies have explored voice liveness detection and authentication methods on headsets or wearable devices [24, 45, 85]. However, most of these works rely on self-developed hardware platforms with heterogeneous microphone layouts and acquisition settings, resulting in non-uniform data distributions. Moreover, neither the collected datasets nor the corresponding hardware implementations are publicly available, which makes fair comparison and reproducibility difficult, as summarized in Table 1.

In contrast, our work introduces a unified multi-microphone smart glasses hardware platform and collects a comprehensive dataset from 42 users, including genuine speech as well as two categories of spoofing attacks. Both the hardware design and the dataset are publicly released, providing the first benchmark specifically targeting voice liveness detection and authentication on smart glasses, to the best of our knowledge.

### 3 AuthGlass Dataset: Comprehensive Passive Acoustic Features for Liveness Detection and Authentication

This section introduces the AuthGlass Dataset that aims for two main objectives: **voice liveness detection** and **authentication** on smart glasses via passive acoustic sensing. Compared with existing datasets for authentication or liveness detection, our dataset offers four key advantages. **(a) Target on Smart Glasses.** To the best of our knowledge, AuthGlass is the first open-source acoustic dataset collected on a smart-glasses form factor for authentication and liveness detection. The dataset captures rich, multi-channel air- and bone-conducted signals from a glasses-mounted sensing platform that coupled with facial anatomy. **(b) Diverse Speakers and Spoofing Scenarios.** AuthGlass includes 42 participants, each providing 15 voice-command samples repeated at six volume levels, capturing substantial intra-speaker variability. The dataset further covers two spoofing categories with multiple attack scenarios, supporting systematic evaluation under diverse adversarial settings. **(c) 16-Channel Synchronized Multimodal Acoustic Capture.** The dataset captures both air- and bone-conducted acoustic signals, totaling 16 synchronized channels. This multimodal design enables the extraction of diverse acoustic features, including speech, vibration, and sound-field cues, and facilitates robust multimodal fusion for wearable authentication. **(d) High-Resolution Data.** Data are collected using a DIY smart-glasses prototype worn naturally by users, with all audio recorded at a 96 kHz sampling rate to preserve fine-grained acoustic details. Replay attacks are generated using high-quality playback devices, resulting in realistic and challenging attack conditions.

In this section, we first review the human articulatory system and examine the acoustic features that smart glasses can potentially capture (Section 3.1). We then identify usable acoustic features through a series of pilot studies (Section 3.2). Next, we describe the authentication and attack models to define the scope and objectives of the dataset (Section 3.3). Finally, we detail the data collection procedure and present a statistical analysis of the AuthGlass dataset (Section 3.4).

#### 3.1 Human Articulatory System and Usable Passive Acoustic Modality

To understand how smart glasses can leverage voice-related features for authentication, it is essential to briefly review the human speech production system, as illustrated in Fig. 2. Airflow from the lungs excites the vocal folds, and the resulting sound source is shaped by the vocal tract into an acoustic signal with characteristic amplitudes and spectral properties [13]. Through precise coordination of the tongue and articulatory muscles, humans produce distinct phonemes, which are further combined to form words and sentences. Crucially, speaker-specific anatomical structures give rise to unique sound propagation paths, resulting in both emitted speech signals and corresponding transmission characteristics that carry user-specific signatures suitable for authentication. Building on this analysis, the acoustic sensing capabilities of smart glasses must be reconsidered under the constraints imposed by their on-body placement and compact form factor. Accordingly, an important question emerges: what types of speech-related cues can be effectively leveraged for liveness detection and authentication on smart glasses?

Research on acoustic liveness detection and speaker authentication for wearables or smart devices [11, 32, 74, 78] has primarily explored four categories of features: (i) voiceprint features extracted from airborne speech, (ii) vibration-related features arising from speech transmission through human skin, (iii) sound field features that characterize the spatial distribution of acoustic energy and phase, and (iv) near-mouth acoustic cues observed in the close-to-microphone region. We hypothesize that smart glasses can capture informative signals of these feature categories.

First, prior studies have demonstrated that voiceprint features essential for speaker authentication can be reliably captured using a single airborne microphone [11]. This modality is naturally compatible with smart glasses, as most off-the-shelf devices already incorporate airborne microphones for voice interaction. Accordingly, in this work, we adopt airborne microphones to capture the primary voiceprint information.

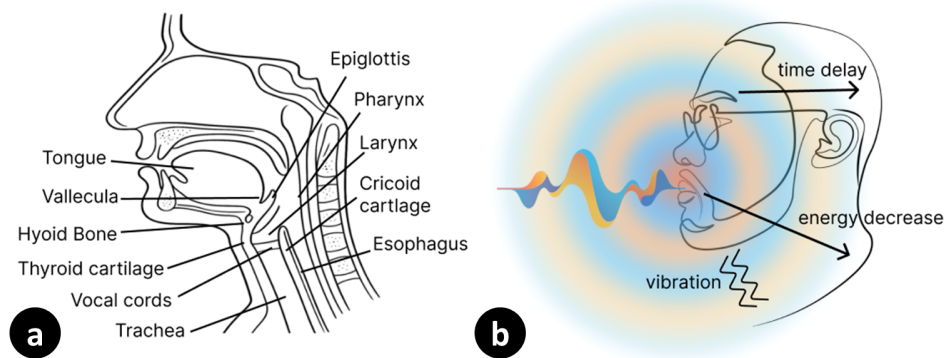


Fig. 2. Human speech production system diagram. (a) Structure of the vocal tract, including the vocal cords, tongue, and other articulatory organs. (b) Acoustic features related to speech production, including vibrations conducted through skin and bones, as well as the spatial propagation effects of the sound field such as time delays and energy attenuation.

Second, prior work [32, 45] has shown that authentication systems relying solely on voiceprint features are vulnerable to spoofing attacks, motivating the use of speech-induced vibration signals as a complementary acoustic modality. Since smart glasses are in direct contact with the user's head, such vibrations can be naturally sensed. Existing studies [24, 62] have explored the use of head-worn IMUs to capture these signals; however, their limited sampling rates (typically below 200 Hz) are insufficient to cover the frequency band of speech production (up to 8 kHz). In contrast, bone-conduction microphones have been shown to capture speech-induced vibrations across the speech frequency range [32]. Based on this observation, we adopt a voice pickup unit (VPU) for vibration-based feature acquisition.

Third, as an alternative approach to strengthening voiceprint-based authentication, sound field features that capture the spatial distribution of acoustic energy and phase have been shown to be effective [78, 81]. The eyeglass frame spans a relatively large area around the head, enabling multiple microphones to be distributed along the frame to sample the surrounding sound field. Indeed, many commercial smart glasses already integrate multiple microphones for audio capture and enhancement [7], demonstrating the practical feasibility of sound field sensing. Building on this insight, we deploy multiple air-conduction microphones on the eyeglass frame to capture sound field information.

Finally, prior studies have shown that close-to-mic acoustic features, such as plosive-related pop sounds [73] and airflow-induced signals [74], can be leveraged for liveness detection and speaker authentication. However, these approaches typically rely on dedicated near-mouth microphones, and the use of such features has not been explored on eyeglass-mounted platforms. We hypothesize that the proximity of the lower rim of the eyeglass frame to the mouth enables the capture of similar close-to-mic acoustic cues. Motivated by the hypothesis, we investigate whether such features can be effectively captured using smart glasses.

To examine the usability of these features, we conduct a series of pilot studies to address the following questions:

- **Air-Conductive Feature (AC):** whether air-conduction microphones deployed on smart glasses can reliably capture user-specific voiceprint information;
- **Vibration or Bone-conductive Feature (BC):** whether bone-conduction microphones can be integrated into smart glasses to acquire vibration signals;
- **Sound Field Feature (SF):** whether multiple air-conduction microphones on smart glasses can capture sound field information, such as spatial variations of acoustic energy and phase;

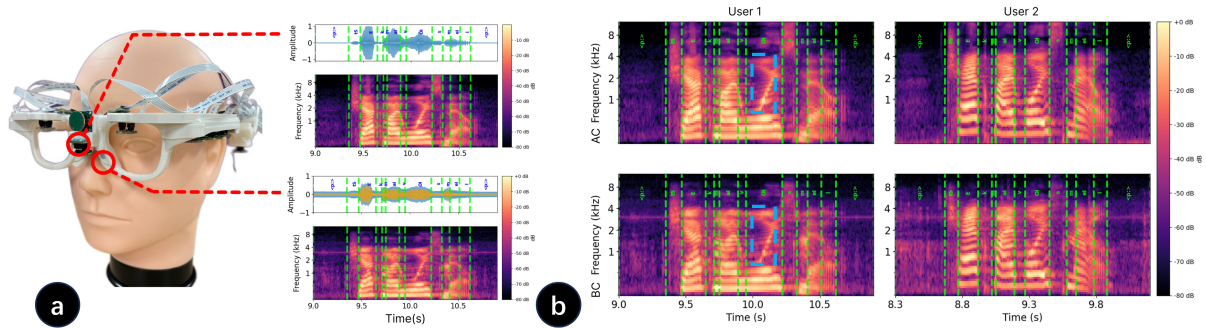


Fig. 3. This figure illustrates the air-conductive (AC) and bone-conductive (BC) microphones used for feature selection. (a) The raw audio signals and corresponding Mel-spectrograms captured by AC and BC microphones when a user speaks the phrase “check my voicemail.” The utterance is segmented into phonemes. The results show that both AC and BC microphones capture rich time–frequency characteristics. (b) Comparison of air-conducted (AC) and bone-conducted (BC) signals from different users uttering “check my voicemail,” visualized using a consistent color scheme. As highlighted by the blue boxes, AC and BC signals from the same user exhibit subtle frequency-related differences, whereas signals captured by either AC or BC microphones show pronounced inter-user variability.

- **Close-to-mic Features:** whether close-to-microphone features can be captured at positions near the mouth on a smart glasses.

### 3.2 Passive Acoustic Feature Selection

Following the preceding questions, we identify usable acoustic modalities through a set of pilot studies. We first built a proof-of-concept smart-glasses frame with microphones mounted at different positions to capture data from multiple acoustic modalities. The pilot study involved three participants, each producing six repetitions of randomly selected passphrases. After data collection, we analyze whether each modality can be used for liveness detection and authentication.

**3.2.1 Study 1: AC features.** To capture air-conducted (AC) features, we mounted an air-conductive microphone at the center of the glasses frame (Fig. 3a). The microphone records audio at a sampling rate of 96 kHz. From the raw recordings, we computed Mel-spectrograms and segmented them at the phoneme level using MAUS [5]. The signal energy is primarily concentrated in the 0–8 kHz range; therefore, we applied an 8 kHz low-pass cutoff. The results indicate that the centrally placed AC microphone captures rich voiceprint-related information, with each phoneme establishing a unique time–frequency pattern. We further compared Mel-spectrograms from two users uttering the same phrase. As shown in Fig. 3b, the AC signals exhibit clear time–frequency differences across users, suggesting that AC sensing on smart glasses can capture discriminative voiceprint features for authentication.

**3.2.2 Study 2: BC features.** Similar to Study 1, we utilized a voice picking unit (VPU) to capture bone-conducted (BC) signals. As the VPU requires direct contact with the human body for data acquisition, we initially placed the sensor on the nose pad and on the inner side of the glasses leg, forming contact with the nose and head, respectively. The results show that when placed on the inner side of the glasses leg, the captured signals are significantly weaker and contain noticeable spike noise. We attribute this to poor contact conditions and potential friction with hair. Based on these observations, we selected the nose pad as the placement location for BC sensing.

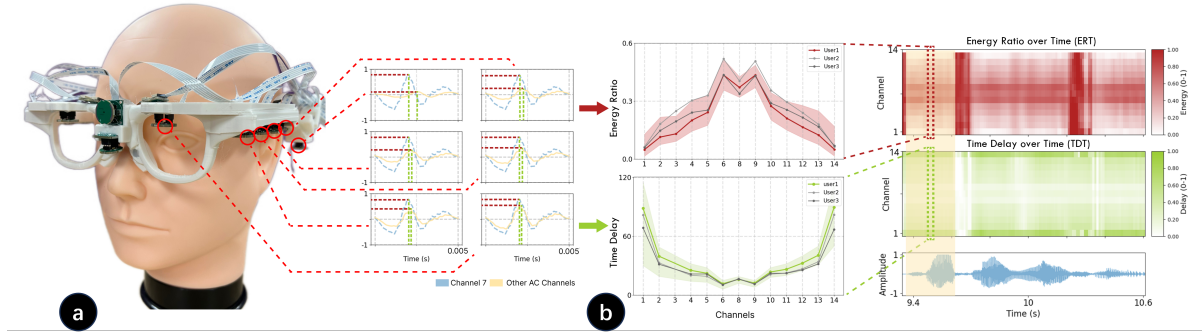


Fig. 4. This figure illustrates the computation of Energy Ratio over Time (ERT) and Time Delay over Time (TDT), along with the spatial acoustic information they capture. (a) Energy attenuation (red dashed line) and time delay (green dashed line) between a selected AC channel and the central AC channel within a short time frame. Both energy attenuation and time delay vary across different AC channels. (b) Normalized energy ratio and time delay distributions across all time frames when a user speaks the phrase “check my voicemail”, forming the ERT and TDT. The left panel shows the averaged energy ratio and time delay distributions of different users, with inter-user variations highlighted by colored regions.

After determining the sensor placement, we used the VPU (96kHz) mounted on the nose pad of the smart glasses to capture bone-conducted data, as shown in Fig. 3a. We analyzed the recorded signals using Mel-spectrograms and segmented them at the phoneme level with MAUS[5]. As shown in Fig. 3b, the VPU on smart glasses captures rich vibration data with time–frequency patterns similar to those of AC signals, while exhibiting subtle but consistent differences in the time–frequency domain, as highlighted by the blue boxes. We applied an 8 kHz cutoff to the BC signals and compared both AC and BC features across two users. Similar to AC signals, BC signals exhibit clear time–frequency differences across users, indicating that BC sensing provides complementary information that can enhance AC-based voiceprint authentication on smart glasses.

**3.2.3 Study 3: SF features.** We further mounted multiple synchronized air-conducted (AC) microphones (96 kHz sampling rate) along the smart-glasses frame to capture sound field features during speech. As shown in Fig. 4a, both energy attenuation and time delays between selected AC channels and the centrally placed AC microphone vary within a short time window. The centrally placed microphone captures the highest energy, while microphones farther from the mouth exhibit reduced energy. These observations indicate that sound-energy decay and phase shifts during acoustic propagation can be captured using spatially distributed AC microphones.

To further extract these features, we segmented the recordings into short time frames. For each frame, we measured the time delay between each selected channel and the central microphone using cross-correlation, and computed the corresponding energy attenuation, as shown in Fig. 4b. To normalize feature distributions across channels, both the time-delay and energy-ratio values were scaled and passed through a hyperbolic tangent function, yielding values in the range  $[-1, 1]$ . Stacking consecutive frames reveals consistent temporal patterns in both energy attenuation and time delay during speech. We denote these features as Channel Energy Ratio over Time (ERT) and Channel Time Delay over Time (TDT) respectively. As shown in Fig. 4b, averaging ERT and TDT along the time axis yields distinctive patterns across the three users, potentially related to individual head geometry.

In addition to time-domain features, we also examined sound-field characteristics in the frequency domain. Inspired by prior work on frequency-domain energy distributions [78, 81], we analyzed channel-wise energy attenuation across frequencies, as shown in Fig. 5 a. Specifically, we applied short-time Fourier transform (STFT)

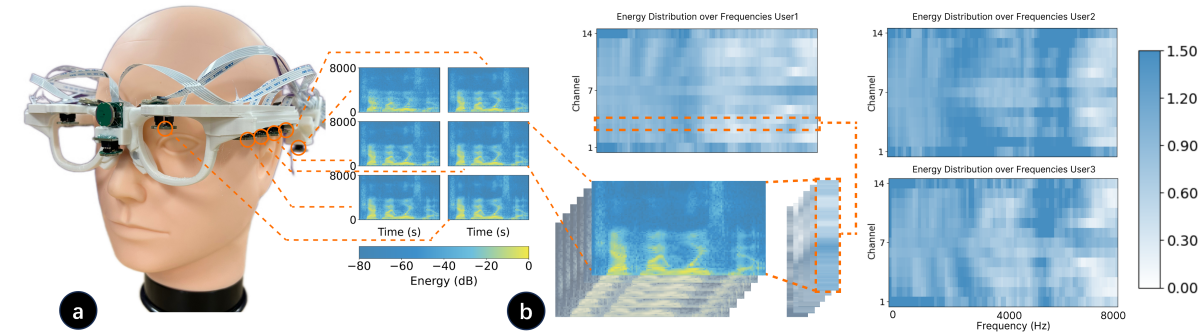


Fig. 5. This figure illustrates the computation of Energy Distribution over Frequencies (EDF) and the spatial acoustic information it captures. (a) STFT of signals recorded by microphones at different positions on the glasses. (b) For each microphone, the STFT is averaged along the time axis to obtain the energy–frequency representation. On the right, EDFs for different users uttering the phrase “check my voicemail” are shown, highlighting inter-user variations.

to the raw signals of each selected channel and averaged the resulting spectra along the time axis to obtain energy–frequency representations. We then computed the energy attenuation between each selected channel and the central microphone within specific frequency bands, and stacked the results across channels, as shown in Fig. 5. The resulting frequency-domain energy distribution exhibits user-specific patterns and inter-user variability, suggesting its potential utility for authentication. We refer to this feature as Channel Energy Distribution over Frequencies (EDF).

**3.2.4 Study 4: Close-to-mic features.** To examine whether close-to-microphone features can be captured using sensors mounted on smart glasses, we placed an airflow sensor and microphones along the lower rim of the eyeglass frame, adjacent to the lenses, to capture airflow and plosive-related pop sounds, following prior works[73, 74]. However, we did not observe discernible close-to-microphone features under this configuration.

**3.2.5 Conclusion.** Based on the above pilot studies, we identify air-conducted (AC), bone-conducted (BC), and sound-field (SF) features as viable passive acoustic modalities for smart glasses authentication. To capture them, a DIY smart glasses prototype is developed with hardware configuration and sensor placement detailed in Section 3.4.1.

### 3.3 Authentication and Attack Model

Here, we illustrate a typical voice-based authentication workflow and its associated attack scenarios on wearable devices, which motivate the design of our dataset collection process. As shown in Fig. 6, a user must enroll a predefined voice passphrase (e.g., “pay the bill”) before use. During enrollment, the system processes the captured audio to generate a user-specific template, which is later used to verify the user’s identity and authorize actions.

During daily usage, the user utters the enrolled passphrase to trigger a command. Upon receiving the audio, the system first performs liveness detection to verify that the command originates from the glasses wearer. If the input passes liveness detection, it is then processed by the authentication model, which compares the input against the stored user template. The command is executed only if authentication succeeds.

This pipeline is subject to several adversarial scenarios. First, the user may speak the passphrase without wearing the smart glasses. In this case, the command should not be triggered, as the device is not actively worn; liveness detection is expected to reject such inputs. Second, when the user is wearing the glasses, an external

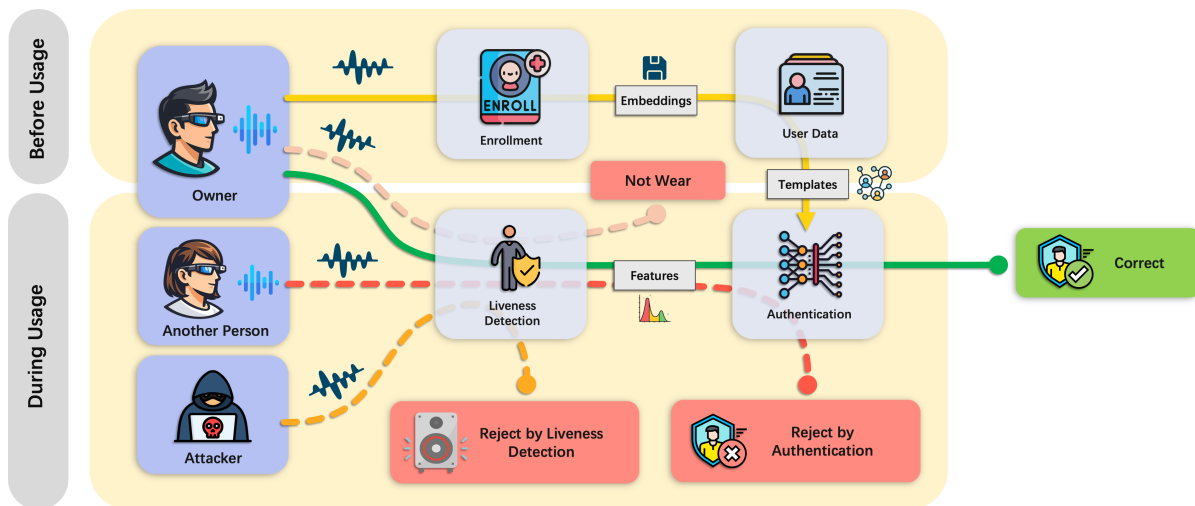


Fig. 6. Workflow of enrollment, liveness detection, and authentication on smart glasses. (a) The yellow path: the enrollment process. After enrollment, an embedding is extracted and stored in the user database as a template for later comparison. (b) The green path: a successful verification, where both liveness detection and authentication are passed. (c) The pink path: user is not wearing the glasses and is rejected by liveness detection. (d) The red path: When another user wears the glasses and attempts verification, they can pass liveness detection but fail authentication. (e) The orange path: When an attacker performs replay or other spoofing attacks, the attempt is rejected by liveness detection.

sound source, such as recorded and replayed audio from the user, may attempt to trigger the command. Similarly, liveness detection should reject these inputs to prevent false activation.

Then, an attacker may gain physical access to the smart glasses and wear them while replaying or producing adversarial audio. In this case, it is more difficult for liveness detection to distinguish the attacker from the genuine user, as the former one provided simulated live inputs. However, the attacker cannot fully mimic the user's biometrics; thus, the liveness detection system should also block this scenario.

Moreover, when another user attempts to authenticate using their own voice, the input will pass through the liveness detection stage, as live audio is received. However, at the authentication stage, the glasses should actively reject the authentication attempt. In real-world scenarios, smart glasses may support multiple users; therefore, the authentication system should allow all enrolled users to be authenticated according to their identities.

From this analysis, we derive two key requirements: (a) liveness detection must reliably accept live inputs from the wearer while rejecting sounds from the surrounding environment; and (b) authentication must discriminate genuine user inputs from those of other users. To benchmark these capabilities across different methods, we define three categories of data:

- **Genuine User Data:** Authentic samples used to evaluate both liveness detection and authentication accuracy. These samples should pass liveness detection and be correctly authenticated or rejected, depending on the task.
- **Replay Attacks from Environmental Sound Sources:** Adversarial samples targeting liveness detection, which should be rejected at this stage.
- **Replay Attacks by Simulated Wearers:** Adversarial samples collected with the attacker wearing the device; these should also be rejected by liveness detection.

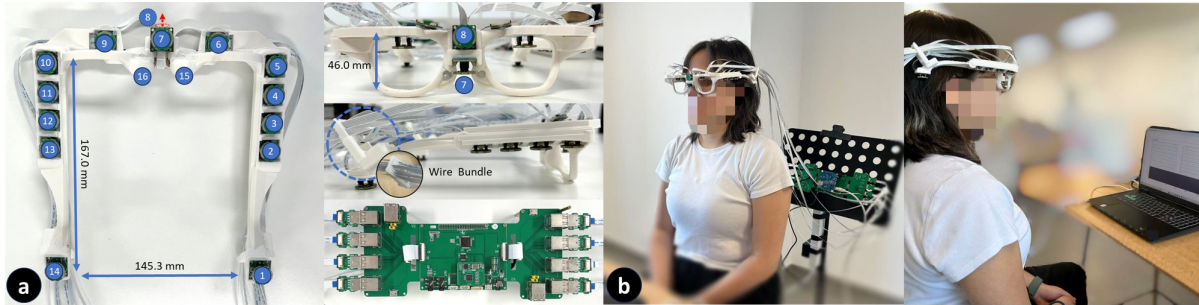


Fig. 7. (a) Structural and hardware overview of the prototype. The system comprises 14 air-conduction microphones and 2 bone-conduction microphones. Each microphone is connected to the data collection board via flexible flat cables, and the temple is designed with a wire bundle, which may introduce crosstalk between channels. (b) Illustration of a user wearing the smart glasses prototype.

### 3.4 AuthGlass Dataset

After identifying the target acoustic modalities and finalizing the data categories, we designed and implemented a DIY smart-glasses prototype and conducted the data collection accordingly. We further analyze the statistical characteristics of the collected dataset.

**3.4.1 Finalize Hardware Implementation.** As discussed in Section 3.2, we select air-conducted (AC), bone-conducted (BC), and sound-field (SF) signals for data collection. To support these modalities, we implement a custom DIY smart-glasses prototype, as illustrated in Fig. 7 a. The prototype integrates 14 omnidirectional AC microphones (Infineon IM73D122V01 [3]) and two voice picking units (VPU14AA01, BC) [8], with an overall frame size of 167.0 mm in length and 145.3 mm in width.

To capture airborne audio from diverse spatial locations and enable sound-field analysis, the AC microphones are distributed along the eyeglass frame and oriented downward. Specifically, five microphones are mounted on each temple, one above each lens, and two at the center of the frame (one facing downward and the other forward) to enrich spatial sampling of the acoustic field.

Guided by insights from the pilot studies, we embed one voice picking unit inside each nose pad to capture BC signals while mitigating potential signal degradation caused by asymmetric skin contact. All microphones are connected via bundled flexible flat cables (FFCs) to a data collection board [10], which supports synchronized acquisition across 16 channels at a sampling rate of 96 kHz. The recorded data are transmitted to a PC over a network connection using the TCP protocol for subsequent processing.

**3.4.2 Data Collection for Authentication and Attack.** Following the authentication and attack models described in Section 3.3, we collected data using our smart-glasses prototype under the three scenarios: genuine usage and two types of replay attacks. The study protocol was approved by the Institutional Review Board (IRB). All data are anonymized for dataset publication.

**Genuine User Data.** We recruited 42 participants (14 female and 28 male), aged 18–42 (mean  $24.6 \pm 4.28$ ), from a university campus. All participants provided informed consent, permitting the use and publication of their anonymized data for research purposes. Data collection was conducted in a quiet conference room to minimize environmental noise. Participants were asked to wear our glasses prototype and were seated in a natural posture and instructed to avoid excessive head or body movements during recording. As illustrated in Fig. 7(b), each participant uttered a predefined set (a total of 15) of voice passphrases (see Appendix A.1) at three distinct volume levels, ranging from soft speech (e.g., speaking to a nearby listener) to loud speech (e.g., projecting to a

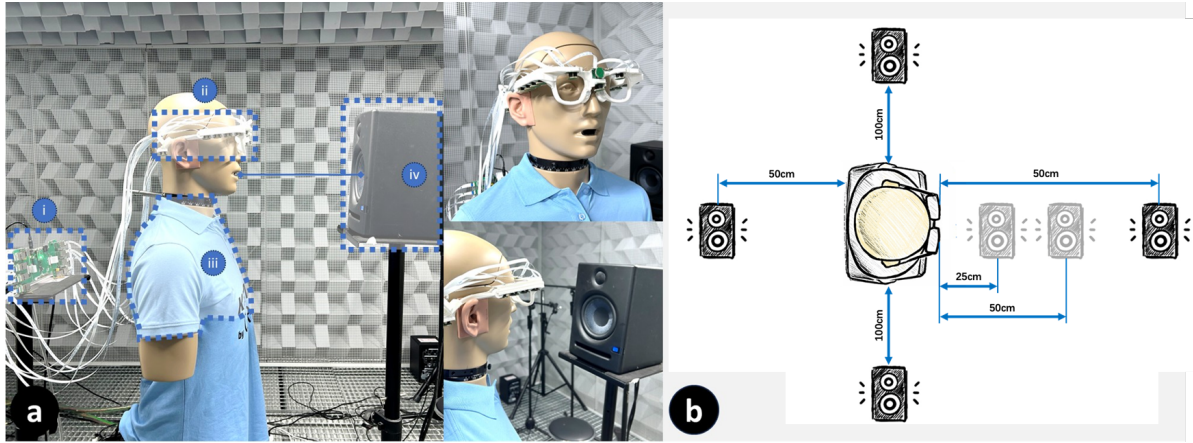


Fig. 8. (a) The environment setting of the voice attack. i is the data collection board and ii is the smart glasses frame. All microphones are connected via bundled flexible flat cables to a data collection board. iii is the torso-mouth simulator and iv is the loudspeaker. In the experiment, two types of attack were applied: loudspeaker replay attacks and a torso-mouth simulator attacks which replicates the exhalation process and torso vibrations during speaking. (b) In the replay attack, the loudspeaker was placed at different positions and distances from the smart glasses to simulate various attack situations.

listener approximately 5 meters away). Each passphrase-volume combination was repeated twice, resulting in six repetitions per sentence. Short rest intervals were provided between passphrases to reduce vocal fatigue. All utterances were captured by the glasses-mounted microphones and manually reviewed to confirm successful recording. The audio was subsequently segmented using MAUS [5], with the resulting segments manually verified for accuracy.

**Replay Attacks from Environmental Sound Sources.** To collect replay attack data under controlled acoustic conditions, we conducted experiments in a sound isolation room, as shown in Fig. 8 a. A mannequin wearing the glasses prototype was used to simulate a stationary user. Genuine utterances were replayed using a high-quality loudspeaker (PreSonus Eris E5 [1]) placed at the same height as the mannequin, with the playback volume manually calibrated to match the sound pressure levels observed during genuine data collection. To model different attack source locations, the speaker was placed at six distinct positions around the mannequin, corresponding to different directions and distances (Fig. 8 b). For each speaker position, all genuine samples were replayed and recorded by the glasses.

**Replay Attacks by Simulated Wearers.** Similar to environmental replay attacks, we collected replay data generated by simulated wearers using a GRAS 45BC KEMAR torso-mouth simulator [2]. The glasses prototype was mounted on the simulator to reproduce realistic head-related acoustics, as shown in Fig. 8 a. All genuine samples were replayed through the simulator's mouth and recorded by the glasses.

**3.4.3 Dataset Statistics.** After data collection, we obtained three datasets, each consisting of 16 synchronized audio channels sampled at 96 kHz. For genuine users, the dataset contains a total of  $42 \times 6 \times 15 = 3,780$  utterances, corresponding to 15 passphrases (length from 2 to 5 words) spoken at three volume levels by each participant. For replay attacks from environmental sound sources, each genuine utterance was replayed and recorded at six distinct speaker locations, yielding  $3,780 \times 6 = 22,680$  attack recordings. For replay attacks by simulated wearers, we collected 3,780 attack samples, matching the size and content of the genuine dataset. All recordings were segmented using MAUS [5] and temporally aligned and segmented, followed by manual verification of

Table 2. Summary of modalities and channel configurations

Modality	Channel	Description
AC	Channel 7	AC channel mounted centrally and facing downward.
BC	Higher-energy channel (15, 16)	Bone-conduction channel with higher signal energy selected as the representative BC input.
SF	Channels [1–6], [8–14]	All remaining AC channels that can function as complementary channels in comparison with the central AC channel.

alignment and segmentation quality. The complete dataset, including raw multichannel recordings, segmentation annotations, and the design files of the smart-glasses prototype, has been publicly released.

#### 4 Benchmarking Voice Liveness Detection and Authentication on Smart Glasses

In this section, we first define the channels corresponding to different acoustic modalities based on our dataset (Section 4.1). We then design a set of benchmark tasks based on the collected data to evaluate voice liveness detection and authentication on smart glasses (Section 4.2). Next, we select seven liveness detection methods and three authentication methods to cover a range of evaluation scenarios (Section 4.3). We further present our proposed lightweight liveness detection and authentication system (Section 4.4). Finally, we report experimental results across all benchmark tasks, showing that our method achieves state-of-the-art performance (Section 4.5) with conclusion (Section 4.6)

##### 4.1 Definition of Acoustic Modalities and Samples Based on AuthGlass Dataset

Among the multi-channel recordings, the air-conducted (AC) microphone mounted on the eyeglass frame and oriented vertically downward (Channel 7 in Fig. 7) consistently provides the highest signal energy and the clearest audio quality among all AC microphones. In addition, the two BC channels capture highly similar signals, the left BC channel (Channel 15) exhibits better signal quality in some samples due to more stable contact conditions. Accordingly, Channel 7 is selected as the representative AC channel, and the BC channel with higher signal quality is selected as the representative BC channel. We define the AC modality as the signal from Channel 7, the BC modality as the selected bone-conducted channel, and the SF modality as the remaining AC channel signals.

For clarity in subsequent discussions, we further categorize the collected data into eight classes. Data collected from the genuine user are denoted as positive samples, while the remaining data are labeled as attack samples (Attack1–Attack7). Detailed definitions of each category are summarized in Table 3.

##### 4.2 Benchmark Tasks Design

We define four benchmark tasks (two for liveness detection and two for authentication) with task description and evaluation metrics, following the authentication and attack model in section 3.3.

**Liveness Detection** aims to determine whether the input audio originates from a genuine glasses wearer. Ideally, it should reject all environmental sounds; however, it may be challenged by inputs from simulated glasses wearers, as such attacks also generate live audio signals. Therefore, we first design a primary liveness detection task that focuses on distinguishing genuine samples from attack samples.

In addition, liveness detection approaches that rely on identifying specific attack devices or synthesized signals may fail to generalize to unseen attacks. This limitation is particularly critical in real-world scenarios,

Table 3. Summary of dataset classes and configurations

Category	Name	Description	Subjects	Utterances / Subject
<b>Genuine User Data</b>	Positive Sample	The genuine user data collected and segmented in section 3.4	42	15 (6 repeats)
<b>Attacks from Wearer</b>	Attack1	The replay data generated by simulated wearers in section 3.4	42	15 (6 repeats)
<b>Attacks from Environment Sound Source</b> with different positions	Attack2	100 cm in front of the user.	42	15 (6 repeats)
	Attack3	100 cm on right side.	42	15 (6 repeats)
	Attack4	100 cm in back of the user.	42	15 (6 repeats)
	Attack5	100 cm on left side.	42	15 (6 repeats)
	Attack6	50 cm in front of the user.	42	15 (6 repeats)
	Attack7	25 cm in front of the user.	42	15 (6 repeats)

where attacks may originate from arbitrary and previously unknown devices. To investigate different methods' performance on this issue, we further design a task to examine the generalization of Liveness Detection to Unseen Attacks.

**4.2.1 Task 1: Liveness Detection Accuracy.** (a) Data Split. To evaluate liveness detection accuracy under different attack methods, we combine positive samples with attack samples from each attack type (Attack 1 to Attack 7), resulting in seven datasets. Each dataset contains an equal number of positive and attack samples from 42 subjects, where attack samples are generated in a one-to-one manner corresponding to the positive samples. For each dataset, we perform a 7-fold cross-validation on subjects, where positive and attack samples are labeled as 0 and 1, respectively.

(b) Method. In each iteration of the cross-validation, six folds of data are used to train the liveness detection model, and the remaining fold is used for testing. The trained model predicts the labels of both positive and attack samples in the test set. Liveness detection performance is measured by the overall classification accuracy on the test data. The accuracy results were averaged across all seven iterations.

**4.2.2 Task 2: Generalization of Liveness Detection to Unseen Attacks.** (a) Data Split. To evaluate the generalizability of liveness detection across different attack types, we first pair the positive samples with attack samples from each attack type (Attack 1 to Attack 7), forming seven separate datasets. For each dataset, we conduct 7-fold subject-level cross-validation, where positive and attack samples are labeled as 0 and 1, respectively, following the same labeling scheme as in the previous task. Importantly, all datasets share the same subject split, ensuring a fair evaluation of cross-attack generalizability.

(b) Method. In each cross-validation iteration, we train the liveness detection model using data from six folds of one dataset, and evaluate it on the remaining fold drawn from each of the other six datasets, measuring prediction accuracy. The final accuracy for that fold is obtained by averaging the results across the six test datasets. For example, in one iteration, samples from subjects 1–36 (six folds) in the (Positive, Attack 1) dataset are used for training. The trained model is then tested on samples from subjects 37–42 (one fold) in each of the (Positive, Attack 2) through (Positive, Attack 7) datasets, producing six accuracy values. These six values are averaged to obtain the accuracy for this fold. This procedure is repeated for all remaining folds (e.g., training on subjects 6–42 and testing on subjects 1–5), and the final performance is reported as the average accuracy across all folds. In our implementation, subject splits are randomly generated but kept consistent across all methods.

**Authentication** aims to distinguish voice inputs from different genuine users by accepting the enrolled user while rejecting all others. Accordingly, we first define a primary authentication task to evaluate the baseline performance of different methods.

In practical scenarios, an authentication system should support fast enrollment with minimal user effort, as requiring repeated utterances for each new voice command is impractical. To reflect this constraint, we further design a task to evaluate authentication performance for cross-utterance scenarios.

**4.2.3 Task 3: Authentication Accuracy.** (a) *Data Split.* To evaluate authentication performance, we conduct a 7-fold subject-level cross-validation. Only positive samples are used, as the task focuses on distinguishing among genuine users. Each sample is labeled with a subject ID (1–42) and an utterance ID (1–15). (b) *Method.* In each cross-validation iteration, six folds are used for training and one fold for testing. The authentication model is trained using raw data along with the corresponding subject and utterance labels. During testing, one sample per utterance is randomly selected from the test fold to form the enrollment set, resulting in 15 enrollment samples per subject. This selection is consistent across all methods. The remaining 75 samples per subject are pooled to form the test set, yielding 450 test samples in total. These samples are then classified by the authentication model to predict the subject identity. Classification accuracy averaged across all iterations is reported as the evaluation metric.

**4.2.4 Task 4: Cross-utterance Authentication Performance.** (a) *Data Split.* To evaluate cross-utterance authentication performance, we follow the same 7-fold subject-level cross-validation protocol as in Task 3. Only positive samples are used, with each sample annotated by a subject ID (1–42) and an utterance ID (1–15).

(b) *Method.* In each cross-validation iteration, six folds are used for training and one fold for testing. The authentication model is trained on the raw data with corresponding subject and utterance labels. During testing, we simulate a cross-utterance enrollment scenario by randomly selecting 5 utterances per subject from the test fold to form the enrollment set. This procedure is repeated three times, covering all 15 utterances per subject in total (i.e., three non-overlapping groups of five utterances). The random selection of utterances for enrollment is fixed and kept consistent across all evaluated methods to ensure a fair comparison. For each repetition, the remaining samples are used as the test set. Authentication accuracy is computed for each repetition, and the average accuracy across the three repetitions is reported as the performance for the current cross-validation iteration. Similar as before, the mean accuracy values are averaged across all iterations.

### 4.3 Existing Method and Adjustments to Multi-channel Acoustic Data

We selected seven representative methods for voice liveness detection and four methods for authentication, spanning AC, BC, and SF acoustic modalities. We further modified these methods to accommodate multiple features, aligning their input formats for systematic comparison.

**4.3.1 Voice Liveness Detection Methods.** We selected seven representative voice liveness detection methods, as summarized in Table 4. These methods span AC, BC, and SF acoustic modalities and employ diverse feature representations and detection models. To enable a fair comparison, we align all methods in terms of input modalities. Below, we briefly introduce each method and describe our corresponding modifications.

**VOID [11]** VOID extracts four types of features from a single-channel AC signal, including three handcrafted features (low-frequency power, signal power linearity, and high-frequency power) and LPCCs. These features are fed into several traditional machine learning classifiers, among which an SVM with an RBF kernel achieves the best performance. To extend VOID to multi-channel inputs, we reapply the entire feature extraction pipeline to each input channel and concatenate all channel-wise features as the input to the SVM classifier.

**He et al. [31]** Similar to VOID, this method extracts five types of features from a single-channel AC signal, consisting of four handcrafted features and LPCCs. The extracted features are input to a self-designed SE-ResNet,

Table 4. Comparison of Voice Liveness Detection Methods

Method	AC	BC	SF	Feature	Model / Method
VOID [11]	✓	-	-	Manually Defined Features	Traditional ML
He et al.(2024) [31]	✓	-	-	Manually Defined Features	CNN
Boneauth [45]	✓	✓	-	MFCC	Cosine Similarity
Eve Said Yes [32]	✓	✓	-	STFT with pooling	Temporal Similarity
Li et al.(2021) [47]	✓	-	✓	STFT with phase	CNN
Cafield [78]	-	-	✓	Fieldprint	GMM
Voshield [81]	-	-	✓	Sound Field Dynamics	CNN
Ours	-	-	✓	TDT and ERT	Cosine Similarity

Table 5. Comparison of Voice Authentication Methods

Method	AC	BC	SF	Feature	Model / Method
Park et al. (2025) [55]	✓	-	-	MFCC	LSTM
Eve Said Yes [32]	-	✓	-	CQT	CNN with AL <sup>1</sup>
Cafield [78]	-	-	✓	Fieldprint	GMM
Voshield <sup>2</sup> [81]	-	-	✓	Sound Field Dynamics	CNN
Ours	✓	✓	✓	MFCC, TDT, ERT and EDF	CNN with AL <sup>1</sup>

<sup>1</sup> indicates methods employing adversarial learning.<sup>2</sup> the method originally do not support authentication.

a residual convolutional neural network (CNN). To support multi-channel inputs, we perform feature extraction independently on each channel and stack the resulting features across channels to form a multi-channel input. We modified the input layer of the SE-ResNet for the multi-channel input.

**Boneauth [45]** Boneauth computes MFCCs from both BC and AC signals and performs liveness detection by measuring the cosine similarity between the two modalities. An input is accepted only if the similarity exceeds a predefined threshold. The threshold is determined by minimizing the Equal Error Rate (EER). Since the original method operates on a single BC–AC pair, we extend it to the multi-channel setting by pairing the BC channel with each AC channel individually and applying majority voting to determine the final liveness decision.

**Eve Said Yes [32]** Eve Said Yes uses pooled STFT energy spectrograms as input features and defines a temporal similarity metric between AC and BC signals for liveness detection. An utterance is accepted if the similarity exceeds a threshold, determined by minimizing EER. As this method also relies on a single AC–BC channel pair, we adopt the same multi-channel voting strategy as used for Boneauth.

**Li et al. [47]** This method is inherently designed for multi-channel voice liveness detection. It leverages both energy and phase spectra derived from STFT as input features and employs a CNN for classification. Since the model naturally accommodates multi-channel inputs, we directly feed features from all selected channels only with the modification on the CNN input layer.

**Cafield [78]** Cafield proposes Fieldprint, a feature computed as the ratio of the energy–frequency relationship vectors between two channels. A GMM is trained to model genuine samples and distinguish them from attack samples. We extend this method by computing Fieldprints between each channel and the reference AC channel (Channel 7), and concatenating all resulting features for GMM-based classification

**Voshield [81]** Voshield utilizes sound field dynamics (SFD), defined as the ratio of STFT spectra between two channels, and employs a residual CNN for binary classification. Similar to Cafield, we compute SFD features between each channel and the reference AC channel (Channel 7), and stack all resulting features as the input to the CNN, with its' input layer modified for all the input channels.

*4.3.2 Voice Authentication Methods.* We selected four voice authentication methods, as summarized in Table 5. Similar to the liveness detection methods, all authentication methods are modified to accommodate multi-channel inputs for a fair comparison.

**Park et al. [55]** This method originally operates on a single AC channel and uses MFCCs as input features. A self-designed LSTM network is employed as the authentication model. During enrollment, embeddings extracted from an intermediate layer are stored as user templates, and cosine similarity is used to compare test embeddings against the enrolled template. Authentication is accepted if the similarity exceeds a predefined threshold. Following this procedure, we compute MFCC features for all selected channels, stack them together, and modify the model input layer accordingly to support multi-channel inputs.

**Eve Said Yes [32]** Eve Said Yes uses CQT features extracted from a single BC channel as input to a residual CNN trained with adversarial learning to produce speaker embeddings. During enrollment, embeddings are extracted from an intermediate fully connected layer and compared with stored templates using cosine similarity. Similar to Park et al., we extend this method by stacking features extracted from all channels and adapting the model input layer to accommodate the expanded multi-feature input.

**Cafield [78]** As discussed previously, Cafield employs a GMM-based framework for both liveness detection and authentication. We apply the same multi-channel feature construction and model modification strategy as used in the liveness detection setting.

**Voshield [81]** Voshield does not originally support authentication, as it is designed for binary liveness classification. However, since it is based on a CNN architecture, it can be readily adapted for authentication by replacing the binary output layer with a fully connected layer followed by a softmax output. We extract embeddings from the fully connected layer immediately following the residual block and perform authentication using cosine similarity, following the same protocol as Park et al. and Eve Said Yes.

#### 4.4 Our Method: AuthG-Live & AuthG-Net

In this section, we detail the implementation of our liveness detection method, AuthG-Live, and our authentication model, AuthG-Net.

*4.4.1 Feature Extraction Implementation.* For feature extraction, log-Mel spectrograms were computed for both air-conduction (AC) and bone-conduction (BC) channels. AC signals were directly transformed into Mel spectrograms, whereas BC signals were first processed using a Butterworth high-pass filter with a cutoff frequency of 100 Hz to suppress movement-induced low-frequency interference and ambient low-frequency noise. All signals were then resampled to 96 kHz via linear interpolation. The Mel spectrograms were generated using 128 Mel filter banks with an upper frequency limit of 8 kHz.

To characterize sound field (SF) properties, we extracted three complementary features: Energy Ratio over Time (ERT), Time Delay over Time (TDT), and Energy Distribution over Frequency (EDF). These features respectively capture spatial sound energy attenuation, inter-channel propagation delays, and the spectral energy distribution across microphones, following the design principles described in Section 3.2.

ERT was computed by applying the short-time Fourier transform (STFT) to each voiced segment and summing the spectral energy within the 100–8,000 Hz band for all air-conducted SF channels (Section 4.1). To eliminate variations caused by sound volume, the energy of each channel was normalized by that of the reference AC

Table 6. Feature Extraction Parameters

<b>Parameters for Mel Spectrogram</b>		
Sampling rate: 96,000 Hz	Maximum frequency: 8,000 Hz	
Hop length: 1024	$N_{FFT}$ : 2048	$N_{MELS}$ : 128
<b>Parameters for ERT and TDT</b>		
Sample rate: 96,000 Hz	Frequency range: 100–8,000 Hz	
Step length: 0.005 s	Scaling factor: 2000	
<b>Parameters for EDF</b>		
Sample rate: 96,000 Hz	Maximum frequency: 8,000 Hz	
Hop length: 1024	$N_{FFT}$ : 1024	

channel (Channel 7). The resulting ratios were linearly scaled and subsequently normalized using a hyperbolic tangent ( $\tanh$ ) function to ensure numerical stability.

TDT is derived by estimating the relative time delay between each air-conducted SF channel and the reference channel (Channel 7) via cross-correlation. For each channel, the time lag corresponding to the peak of the correlation function is selected as the delay estimate. A confidence score is then computed by normalizing the peak correlation with the signal energies and applying a logit-like transformation. The final time delay is obtained by weighting the estimated lag with its confidence score, thereby suppressing unreliable measurements caused by absent inputs or noise while preserving robust delay estimates. Consistent with ERT, the resulting values are linearly scaled and further normalized using a  $\tanh$  function to ensure numerical stability.

EDF was computed by applying STFT to each voiced segment across all channels. For each air-conducted channel, the resulting energy spectrogram was averaged along the time dimension to obtain a frequency-wise energy distribution. Channel 7 was again selected as the reference, and the remaining air-conducted channels were normalized by the maximum STFT energy of the reference channel. This normalization preserves relative spectral energy distributions across frequency bands while mitigating variations in overall signal amplitude. A summary of all feature parameters is provided in Table 6.

**4.4.2 AuthG-Live: Attack Device Independent Voice Liveness Detection.** Most existing voice liveness detection methods learn discriminative patterns from attack samples observed during training [11, 31]. As a result, their generalization performance strongly depends on the diversity of attack types seen during training. When confronted with unseen spoofing techniques or replay configurations, detection accuracy often degrades, leading to reduced robustness in real-world deployments. Furthermore, constructing such systems requires collecting and annotating audio under diverse attack devices, environments, and playback settings, which incurs substantial cost—particularly for smart glasses, where large-scale datasets are scarce.

In contrast, AuthG-Live is a generalizable voice liveness detection framework that leverages the physical characteristics of human sound propagation rather than attack-specific artifacts. Specifically, it models the near-source spatiotemporal sound field by extracting Energy Ratio over Time (ERT) and Time Delay over Time (TDT) from multi-channel air-conducted signals, capturing intrinsic source–vocalization relationships that are difficult for replay or synthesized attacks to replicate. Importantly, AuthG-Live is trained solely on genuine speech data, eliminating the need to enumerate diverse attack scenarios and thereby enabling robustness against unseen spoofing methods. Moreover, the proposed features can be extracted in a streaming manner, supporting real-time sound field analysis and rapid attack detection, which makes the framework well suited for on-device deployment in practical wearable applications.

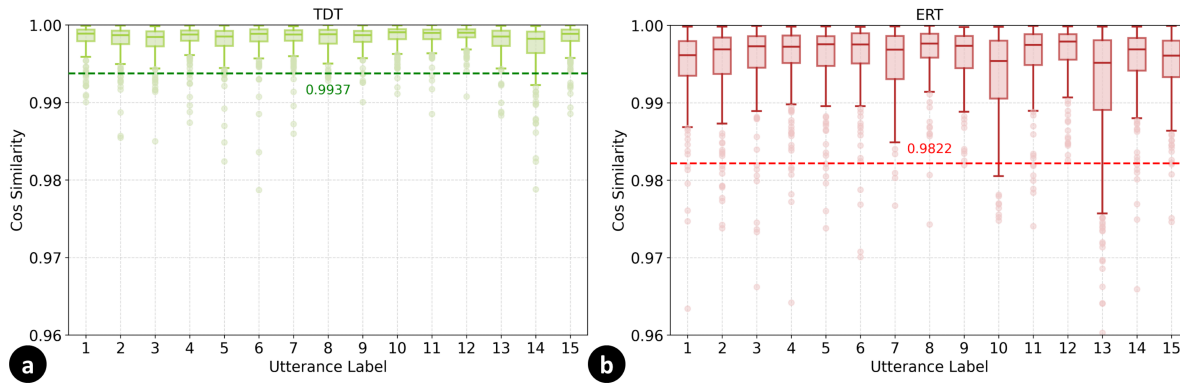


Fig. 9. This figure shows the distribution of cosine similarities between the unified patterns and the corresponding aTDT and aERT across all genuine samples for the 15 utterances. Each box in the boxplot represents the interquartile range (25th to 75th percentile), with the line inside indicating the median. Scattered points denote outliers, and the dashed line marks the 3rd percentile of the genuine similarity distributions. In (a), the TDT cosine similarity between aTDT and the unified patterns defines a threshold of 0.9937, whereas in (b), the ERT yields a threshold of 0.9822.

To this end, we incorporate TDT and ERT, as these features reflect the spatial origin of the received signals. Specifically, TDT and ERT are averaged along the time axis for each channel to form mean templates, denoted as aTDT and aERT, which summarize sound propagation delay and energy attenuation patterns.

For liveness detection, the aTDT and aERT from genuine user samples are averaged to obtain unified aTDT and aERT patterns. These two unified patterns represent the typical acoustic propagation behavior of genuine speech. Given an input signal, its corresponding aTDT and aERT are computed and compared with the unified patterns using cosine similarity. A similarity score exceeding a predefined threshold indicates that the signal is likely emitted from a real human speaker.

To determine the decision threshold, we compute the cosine similarity between the unified patterns and the corresponding aTDT and aERT extracted from all genuine samples. The results exhibit consistently high similarity across utterances and subjects. Accordingly, the thresholds are set based on the 3rd percentile of the genuine similarity distributions, allowing 97% of genuine samples to be accepted. This data-driven criterion ensures a high true acceptance rate for genuine speech while effectively rejecting most spoofing attacks. As illustrated in Fig. 9, the resulting similarity thresholds are 0.9937 for aTDT and 0.9822 for aERT. An input signal is classified as live only if both similarity scores exceed their respective thresholds.

**4.4.3 AuthG-Net: Passphrase-Independent Voice Authentication.** AuthG-Net is a lightweight deep learning model designed for user authentication, as illustrated in Fig. 10. It takes AC, BC, and SF modalities as input. Each modality is first processed by an individual CNN encoder to extract early embeddings, which are then concatenated for feature fusion. The fused representation is further processed by a ResNet-18 backbone to obtain a discriminative user embedding. This embedding is finally fed into two parallel heads, enabling cross-utterance learning and allowing the enrolled passphrase to generalize to unseen passphrases.

For the AC and BC modalities, we use mel-log spectrogram features as described in Section 4.4.1. To ensure consistent input sizes, all inputs are padded with zero to a fixed shape of (215, 128), which is selected to cover the maximum time duration of all samples. These features are passed to their corresponding encoders, each consisting of a 2D convolution layer with a  $3 \times 3$  kernel, stride 1, and 32 output channels for early feature extraction. We adopt

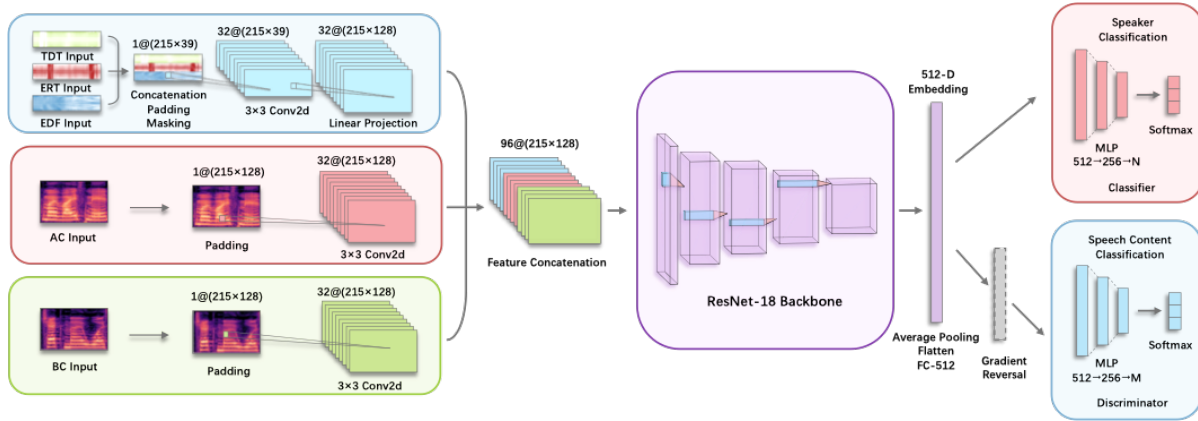


Fig. 10. The figure demonstrate the architecture of AuthG-Net. The blue/red/green blocks on the left denote the SF/AC/BC inputs, which are encoded by lightweight CNN heads and then stacked and fed into a ResNet-18 backbone (purple block) to produce a 512-D embedding. In the domain-adversarial learning (DAL) branch, the model is optimized with two objectives: speaker classification (red) and speech-content classification (blue). The speaker classifier is trained directly on the embedding, whereas the passphrase classifier is connected via a Gradient Reversal Layer (GRL), which reverses gradients during backpropagation to encourage content-invariant embeddings.

the same encoder design for AC and BC features since they are extracted using identical mel-log spectrogram settings. ReLU activation functions are applied in each layer to facilitate non-linear representation learning.

For the SF feature input, TDT, ERT, and EDF are jointly used. To align the encoded feature shapes with those from AC and BC, all SF features are padded to the same temporal length. TDT and ERT naturally share the same length as the corresponding AC and BC features; therefore, they are padded using the same procedure, resulting in a shape of  $(215, 13)$ . Since TDT can produce unstable values when input signals are absent, we compute the energy from the AC signal and mask TDT frames whose energy falls below a predefined threshold. This is feasible because SF features are derived from AC signals. For EDF, whose original shape is  $(86, 13)$ , we apply linear scaling to resize it to  $(215, 13)$ , matching the temporal length of AC and BC features.

After pre-processing, TDT, ERT, and EDF features are concatenated along the temporal axis and passed through a 2D convolution layer with a  $3 \times 3$  kernel, stride 1, and 32 output channels. The resulting feature map is then processed by a linear projection layer to project the width dimension to 128, matching the embedding shapes of the AC and BC features. Similar to the AC and BC encoders, ReLU activation functions are employed in each layer to enable non-linear processing.

To fuse the embeddings from the AC, BC, and SF encoders, we concatenate the three encoded features along the channel axis, resulting in a 96-channel fused representation. This fused feature is then fed into a ResNet-based backbone that incorporates all four residual blocks, with the first convolution layer modified to accommodate the increased channel size. After average pooling and flattening, the backbone outputs a 512-dimensional embedding that represents the user feature and is used for downstream classification during training.

To encourage passphrase-independent speaker verification, we adopt a domain adversarial learning (DAL) framework [27, 71] with two learning objectives: speaker classification and speech-content classification. Both classifiers consist of three fully connected layers followed by a softmax output. The speaker classifier is optimized directly on top of the embedding, while the content classifier is connected through a Gradient Reversal Layer (GRL), which reverses gradients during backpropagation to adversarially suppress content-related information in the learned embedding. Following the DAL formulation, the overall loss function is defined as:

Table 7. Comparison on Liveness Detection Accuracy with All Acoustic Modalities under Different Attacks.

Attacked by	Attack 1	Attack 2	Attack 3	Attack 4	Attack 5	Attack 6	Attack 7
VOID	99.09%	99.10%	99.19%	99.02%	98.84%	98.93%	98.45%
He et al. (2024)	99.91%	<b>100.00%</b>	99.96%	<b>100.00%</b>	<b>100.00%</b>	<b>100.00%</b>	99.96%
Boneauth	91.80%	90.58%	85.52%	94.10%	95.04%	85.67%	79.60%
Eve Said Yes	20.95%	55.70%	85.82%	66.10%	61.24%	40.08%	26.93%
Li et al. (2021)	<b>100.00%</b>	<b>100.00%</b>	97.22%	<b>100.00%</b>	<b>100.00%</b>	<b>100.00%</b>	<b>100.00%</b>
Cafield	76.87%	<b>100.00%</b>	<b>100.00%</b>	<b>100.00%</b>	<b>100.00%</b>	<b>100.00%</b>	<b>100.00%</b>
Voshield	99.99%	99.99%	<b>100.00%</b>	<b>100.00%</b>	<b>100.00%</b>	<b>100.00%</b>	<b>100.00%</b>
Ours	76.41%	96.67%	96.67%	96.67%	96.67%	96.67%	96.67%
Ours (Optimized 6 channels) <sup>1</sup>	96.26%	96.79%	96.79%	96.79%	96.79%	96.79%	96.77%

<sup>1</sup> Optimization is described in section 5.3.

<sup>2</sup> Since the other methods are trained and evaluated using known attack types, they may be prone to overfitting to specific attacks. In contrast, our method determines the decision threshold using only genuine samples and demonstrates superior performance under unseen attack scenarios, as discussed in Section 4.5.2.

$$L(w_f, w_s, w_p) = L_s(w_f, w_s) - \lambda \cdot L_p(w_f, w_p)$$

where  $L_s$  and  $L_p$  denote the cross-entropy losses for speaker classification and passphrase classification, respectively, and  $\lambda$  is set to 1. Here,  $w_f$ ,  $w_s$ , and  $w_p$  represent the parameters of the feature extractor, speaker classifier, and passphrase classifier.

During training, samples are provided with both subject labels and utterance labels. The training process is formulated as a classification task, encouraging the model to learn utterance-independent and user-related representations. We use the Adam optimizer for model optimization. After training, the output of the embedding layer (highlighted in purple in Fig. 10) is used as the user feature. During enrollment, this feature is extracted and stored as the user template. During authentication, the stored template is compared with the extracted feature using cosine similarity. If the similarity score exceeds a predefined threshold, the input is accepted as originating from the enrolled user.

## 4.5 Results and Analysis on Benchmark Tasks

In this section, we provide result and analysis on the benchmark tasks defined in section 4.2

**4.5.1 Task 1: Liveness Detection Accuracy.** We firstly conducted benchmark Task 1 on all selected liveness detection methods. The results are summarized in Table 7. We also implemented the original version of the selected methods with analysis provided in appendix A.2. As shown in the table, our method using all SF modality inputs achieves high liveness detection accuracy from Attack 2 to Attack 7, indicating that the proposed method can reliably detect replay attacks from the environment.

However, for Attack 1, i.e., the simulated wearer attack, the accuracy using all SF channels only reaches 76%, which suggests that the simulated wearer can, to a certain degree, mimic the sound source position of a genuine user. Further analysis in section 5.3 reveals that this performance degradation is mainly caused by the fact that some channels are insensitive to sound source position when relying on time delay and energy ratio cues. By incorporating only the channels that are sensitive to sound source position, our method achieves a significantly improved liveness detection accuracy of over 96%.

Table 8. Comparison on Generalizability of Liveness Detection by the Averaged Accuracy for Unseen Attacks.

Trained by	Attack 1	Attack 2	Attack 3	Attack 4	Attack 5	Attack 6	Attack 7
VOID	52.11%	87.13%	64.74%	64.92%	61.95%	90.90%	89.41%
He et al. (2024)	60.38%	90.36%	77.89%	74.38%	72.44%	90.70%	77.87%
Boneauth	70.45%	78.16%	72.58%	52.34%	65.40%	81.23%	82.48%
Eve Said Yes	46.61%	49.64%	50.99%	47.73%	50.19%	47.80%	46.96%
Li et al. (2021)	68.37%	90.13%	60.26%	65.21%	63.45%	87.27%	91.16%
Cafield	89.61%	94.12%	94.12%	94.12%	94.12%	94.12%	94.12%
Voshield	<b>99.98%</b>	92.33%	92.75%	70.82%	78.98%	92.49%	82.62%
Ours <sup>1</sup>	93.78%	93.78%	93.78%	93.78%	93.78%	93.78%	93.78%
Ours (Optimized 6 channels) <sup>2</sup>	96.71%	<b>96.71%</b>	<b>96.71%</b>	<b>96.71%</b>	<b>96.71%</b>	<b>96.71%</b>	<b>96.71%</b>

<sup>1</sup> As our method do not require attack samples for training, we average the liveness detection accuracy on all attacks.

<sup>2</sup> Optimization is described in section 5.3.

Although several baseline methods report accuracy values close to or even reaching 100%, we suspect that this performance gain mainly comes from learning device-specific characteristics of the attacking loudspeaker rather than intrinsic liveness cues. Since only a single attack type is involved in both training and testing for each experiment, it becomes relatively easy for the model to distinguish attacks based on device-related features. As will be shown in the subsequent liveness detection generalizability experiments, the performance of such methods degrades significantly when unseen attack samples are introduced.

Moreover, we would like to point out that *Eve Said Yes*, a method relying on loose similarity between AC and BC modalities, fails to distinguish between genuine and attack samples. This is because airborne signals can also induce vibrations on the BC sensors, resulting in BC signals that are highly correlated with AC signals. In addition, for the simulated wearer attack, similar AC and BC signal patterns can be generated, which further increases the difficulty of reliable discrimination.

**4.5.2 Task 2: Generalization of Liveness Detection to Unseen Attacks.** We then conducted Task 2 to further evaluate the generalizability of the liveness detection methods by training on one type of attack and testing on other attack types. The results are shown in Table 8. Noticeably, the liveness detection accuracy of all current methods degrades when facing unseen attacks, with methods that solely rely on attacker-device-related features suffering the most severe degradation (e.g., VOID and He et al.).

By applying a strict similarity metric on the AC and BC modalities, Boneauth still retains part of its capability in detecting attacks. However, it also exhibits noticeable performance degradation (from around 90% to around 75%) as the thresholds across different attack types are determined by corresponding EER, thus become inconsistent. *Eve Said Yes* completely fails to distinguish unseen attacks from genuine samples, resulting in an accuracy of around 50%. In contrast, methods that rely on SF modalities (Li et al., Cafield and Voshield) show less degradation, indicating that sound field features can potentially support cross-attack detection, as they do not depend on specific attack-device-related characteristics.

Among Li et al., Cafield, Voshield, and our method, ours with optimization achieves the highest accuracy with stable performance across all seven attack types, while the other three suffer from accuracy degradation under one or more attacks. The method proposed by Li et al., which incorporates original STFT spectrograms, inevitably learns attack-device-specific features that cannot generalize to other attack scenarios, leading to the most severe performance degradation (more than 30%) compared to Cafield and Voshield. Although the latter two methods incorporate only SF-related features without using original signal representations, they still rely on

Table 9. Authentication results for Benchmark Task 3 and Task 4 with original and extended implementations.

Method	Benchmark Task 3 (15 utterance enroll)		Benchmark Task 4 (5 utterance enroll)	
	Origin	Extended	Origin	Extended
Park et al	71.11%	80.24%	69.68%	78.38%
EVE said Yes	80.74%	88.63%	78.33%	87.08%
Cafield	74.82%	75.23%	67.76%	70.90%
Voshield	83.97%	96.21%	81.88%	93.17%
Ours	–	<b>97.95%</b>	–	<b>96.93%</b>

CNN-based models that require both attack and genuine samples during training, and therefore cannot generalize well to unseen attacks. In contrast, our method requires no attack samples for training and only leverages a static similarity-based comparison, enabling robust performance when facing unseen attacks.

**4.5.3 Task 3: Authentication Accuracy.** Next, we conducted Task 3 to evaluate the authentication performance of the selected baseline methods and our proposed approach, as shown in Table 9. Notably, our method achieved the best performance among all compared methods, indicating that the proposed feature extraction strategy together with AuthG-Net can effectively capture user-related characteristics.

The method proposed by Park et al. leverages an LSTM and a randomized embedding generation scheme, but it is designed only for single-user scenarios. As a result, it cannot effectively learn discriminative embeddings for multiple users, leading to limited capability in capturing user-related features and consequently a low authentication accuracy (80.24%).

Although Eve Said Yes supports embedding extraction for different inputs, its model struggles to extract and fuse features from multiple modalities, resulting in only limited improvement in authentication performance (from 80.74% to 88.63%). Cafield leverages the fieldprint sound field (SF) feature, yet exhibits poor performance under both the original and extended implementations. This may be attributed to the limited modeling capacity of the GMM-based classifier. In contrast, Voshield, which adopts the SFD feature, achieves an accuracy close to that of our method, with an improvement of approximately 13% compared to its original implementation. This suggests that the CNN-based architecture in Voshield is effective at extracting discriminative representations from different acoustic features.

**4.5.4 Task 4: Cross-Utterance Authentication Performance.** Finally, we conducted Task 4 to evaluate authentication performance under cross-utterance settings. As shown in table 9, our method continues to achieve the best authentication performance, with only a slight degradation of around 1% compared to Task 3. This result indicates that the proposed method can effectively learn utterance-independent user-related features, benefiting from the design of DAL.

In contrast, the other four methods experience varying degrees of performance degradation, with Cafield and Voshield being particularly affected (5% and 3%, respectively). This is likely because the sound field features they leverage (fieldprint and SFD) are closely related to the utterance content itself, as different phonemes may exhibit distinct sound field characteristics. Moreover, since our method separately processes sound field features in the frequency domain (EDF) and time domain (ERT and TDT), it demonstrates stronger generalizability across different utterances.

For the methods proposed by Park et al. and Eve Said Yes, although their original authentication performance is relatively limited, the performance degradation under cross-utterance settings is comparatively small (around 1% to 2%). This suggests that these methods are able to extract utterance-independent features to some extent.

## 4.6 Conclusion

In conclusion, our method achieves state-of-the-art performance in both voice liveness detection and authentication. It demonstrates strong generalization capability for liveness detection against unseen attacks, as well as robust performance in cross-utterance authentication scenarios.

## 5 Evaluation

Considering that our method is developed using relatively high-quality equipment to facilitate theoretical analysis, it is essential to validate its effectiveness under practical constraints. To this end, we systematically evaluate the system performance through a series of ablation studies. Specifically, we first investigate the impact of reduced sampling rates, rather than using the original 96 kHz setting (Section 5.1). We then examine the system performance under limited acoustic modalities, instead of jointly leveraging AC, BC, and SF modalities (Section 5.2). Furthermore, we explore configurations with a reduced number of SF channels, as employing 14 AC microphones is impractical for real-world smart glasses (Section 5.3). Finally, we simulate the microphone layouts of two off-the-shelf products, Rokid [7] and Meta Ray-Ban [6], and evaluate the liveness detection and authentication performance of our method under these realistic settings (Section 5.4).

### 5.1 Limited Sampling Rate

Our prototype records audio at a high sampling rate of 96 kHz. In contrast, most commercial smart glasses adopt microphones with a sampling rate of around 16 kHz. To investigate the effect of sampling rate on the performance of the authentication system, we evaluated the model under four different sampling rates: 16 kHz, 32 kHz, 48 kHz, and 96 kHz. To simulate the characteristics of lower-rate microphones, the original recordings were first decimated on each channel using FIR-based low-pass filtering, followed by uniform downsampling to the target frequency. While a reduced sampling rate has minimal impact on Mel-spectrogram computation, it can influence sound field modeling, which relies on precise temporal information. Therefore, to enable low-rate recordings to approximate the temporal resolution required by higher-rate processing pipelines, the downsampled signals were linearly interpolated, preserving the bandwidth constraints imposed by the lower sampling rate while recovering a denser temporal representation. The processed signals were then used for feature extraction and subsequent evaluation, following Benchmark Task 1 (Liveness Detection Accuracy) and Benchmark Task 3 (Authentication Accuracy) detailed in Section 4.2. All AC, BC and SF modalities are used for liveness detection and authentication. The results of these experiments are summarized in Table 10 for liveness detection and Table 11 for authentication.

*5.1.1 Results and Discussion.* As shown in Table 10, the original implementation of the AuthG-Live method with all SF modality channels exhibits high and robust liveness detection accuracy on attack2 to attack7 (all above 96%), with no apparent performance degradation as the sampling rate decreases. However, the original AuthG-Live method fails to effectively discriminate attack1, and the accuracy decreases from 76% to 66% when the sampling rate is reduced from 96 kHz to 16 kHz. Despite this limitation, our method can be optimized (Section 5.3) by selecting only the air-conducted channels in the SF modality that are sensitive to the speaker sound source position. With this optimized design, AuthG-Live achieves robust liveness detection performance against all seven attacks across different sampling rates, with accuracy consistently higher than 95%. For authentication accuracy, as shown in Table 11, our proposed method, AuthG-Net, maintains accurate authentication performance with an accuracy higher than 97.93%, despite the decrease in sampling rate.

### 5.2 Limited Acoustic Modalities

Though our glasses prototype supports simultaneous capture of AC, BC, and SF modalities, this is not the case for some smart glasses products, as they may not incorporate bone-conducted microphones (or voice picking

Table 10. Comparison on Liveness Detection Accuracy under Different Sampling Rates and Input Channels.

Input Channels	Sampling Rate	Attack 1	Attack 2	Attack 3	Attack 4	Attack 5	Attack 6	Attack 7
AuthG-Live	16 kHz	66.40%	96.76%	96.76%	96.76%	96.76%	96.76%	96.76%
	32 kHz	73.91%	96.69%	96.69%	96.69%	96.69%	96.69%	96.69%
	48 kHz	75.63%	96.67%	96.67%	96.67%	96.67%	96.67%	96.67%
	96 kHz	76.41%	96.67%	96.67%	96.67%	96.67%	96.67%	96.67%
AuthG-Live (Optimized) <sup>1</sup>	16 kHz	95.67%	96.72%	96.72%	96.72%	96.72%	96.72%	96.69%
	32 kHz	96.22%	96.77%	96.77%	96.77%	96.77%	96.77%	96.75%
	48 kHz	96.15%	96.72%	96.72%	96.72%	96.72%	96.72%	96.71%
	96 kHz	96.26%	96.79%	96.79%	96.79%	96.79%	96.79%	96.77%

<sup>1</sup> Optimization is described in section 5.3.

Table 11. Authentication results under Different Sampling Rates.

Sampling Rate	16 kHz	32 kHz	48 kHz	96 kHz
Accuracy	98.52%	97.93%	98.44%	97.95%

units), or they may not incorporate multiple microphones for SF modality capture. Whether our method could be generalized and remain useful with limited acoustic modalities remains unknown.

To evaluate this, we consider representative modality combinations (modalities are defined in Section 4.1). Since AC modality is primary for voice authentication, while BC and SF modalities act as complementary features, we define four combinations: single AC modality, AC and BC modalities combined, AC and SF modalities combined, and the combination of all AC, BC, and SF modalities. Since our AuthG-Live method relies solely on the SF modality and cannot be tested without SF microphone channels, we only experiment on the authentication accuracy of AuthG-Net following Benchmark Task 3, as detailed in Section 4.2. The sampling rate is 96kHz.

To support reduced modality inputs, we implement three additional corresponding variants based on our proposed AuthG-Net to accommodate different modality combinations. This is straightforward to implement, since the encoders for different modalities are separated, and we only need to remove the corresponding modality encoder while retaining the others before feature fusion. For example, in the AC+SF combination experiment, we retain only the AC and SF encoders for feature fusion and remove the BC encoder. For single AC input, the proposed AuthG-Net method degrades to a residual CNN network with DAL.

We also implement Voshield for comparison. Since it achieves the second-highest accuracy based on the results in Section 4.5.3, we implement three variants of Voshield to accommodate reduced modality inputs, following the same modification principle described in Section 4.3.

**5.2.1 Results and Discussion.** As shown in Table 12, the results indicate that reducing the available acoustic modalities degrades authentication performance for both our method and the baseline model. This suggests that BC and SF features can effectively serve as complementary features for voice authentication. Moreover, our model achieves higher authentication accuracy than the baseline when combining AC features with either SF or BC features, validating that the proposed AuthG-Net can effectively extract user-related features from BC and SF modalities, and fuse the feature from AC modality. Nevertheless, even with only a single AC input, our method

still achieves an accuracy of 91.83%, which is higher than that of the baseline. This demonstrates that our design remains effective and generalizable under degraded modality conditions.

Table 12. Authentication results under Different Acoustic Modalities.

Acoustic Modalities	AC	AC+BC	AC+SF	AC+BC+SF
Voshield	79.52%	87.86%	95.24%	96.21%
Ours	91.83%	97.64%	95.71%	97.95%

### 5.3 Limited Input Channels and Optimization on Channel Selection

After validating that our proposed method can generalize to different modality combinations, we further explore its performance under limited input-channel settings. This investigation is motivated by the fact that only a few off-the-shelf smart glasses are equipped with multiple microphone inputs. While in practical scenarios, the number of available microphone channels is constrained by factors such as power consumption, device weight, and user comfort.

In this section, we examine whether using a limited number of microphones can achieve competitive—or even improved—performance in both liveness detection and speaker authentication compared with the full-channel configurations based on our dataset. Specifically, we study the impact of the number of air-conduction microphones and their placement, as well as the effect of incorporating bone-conduction microphones on overall system performance.

Common smart glasses equipped with multiple microphones usually incorporate 3 to 5 channels of AC microphones. Accordingly, we consider three representative setups for evaluation: a 4-channel array, as in Rokid [7]; a 5-channel array, as in Ray-Ban Meta [6]; and a 7-channel array, which is potentially feasible given the spatial layout of our prototype. For each case, we first optimized the microphone placement for liveness detection using AuthG-Live. Considering that current commercial smart glasses typically adopt symmetric microphone layouts, we primarily focus on symmetric configurations during optimization, while also exploring potentially optimal asymmetric layouts for liveness detection.

During layout optimization, Channel 7 was selected as the input for the AC modality. For the 4-, 5-, and 7-channel configurations, all possible combinations of the remaining air-conduction channels were evaluated for liveness detection, following the procedure of Benchmark Task 1 described in Section 4.2. For each configuration, both the best-performing symmetric and asymmetric layouts were identified.

After optimizing the AC microphone layouts, we further evaluated speaker authentication performance using the corresponding optimized configurations, with and without BC microphones. This evaluation follows the procedure of Benchmark Task 3 described in Section 4.2. To enable AuthG-Net to accommodate different numbers of SF input channels, we modify the input channel dimension of the projection layer in the SF feature encoder. Optional BC inputs are incorporated using the same approach described in Section 5.2. The sampling rate is 96kHz.

**5.3.1 Results and Discussion.** The detailed optimized channel configurations are illustrated in Fig. 11. As shown in the figure, air-conducted microphones placed behind the ear are selected across all configurations, indicating that this position is more sensitive to capturing variations in time delay and energy ratio due to its farthest distance from the mouth.

Table 13 presents the liveness detection accuracy for all optimized channel configurations. For all microphone setups, the detection accuracy for Attack 2 to Attack 7 exceeds 96%, indicating that AuthG-Live can robustly detect

Table 13. Comparison on Liveness Detection Accuracy under Different Input Channels.

Layout	Input Channels	Attack 1	Attack 2	Attack 3	Attack 4	Attack 5	Attack 6	Attack 7
symmetric	5 channels	93.56%	96.89%	96.89%	96.89%	96.89%	96.89%	96.89%
	7 channels	94.22%	96.77%	96.77%	96.77%	96.77%	96.77%	96.77%
asymmetric	4 channels	94.55%	96.92%	96.92%	96.92%	96.92%	96.89%	96.92%
	5 channels	94.84%	96.85%	96.85%	96.85%	96.85%	96.85%	96.85%
	7 channels	96.26%	96.79%	96.79%	96.79%	96.79%	96.79%	96.77%

Table 14. Authentication results under Different Input Channels.

Layout	Symmetric		Asymmetric			
	Input Channels	5 Channels	7 Channels	4 Channels	5 Channels	7 Channels
AC+SF		94.13%	94.60%	93.31%	94.15%	95.80%
AC+BC+SF		97.94%	97.45%	97.83%	96.76%	97.94%

attacks originating from environmental sound sources. For Attack 1, only the 7-channel asymmetric configuration achieves a detection accuracy higher than 96%, while the remaining configurations yield accuracies of around 93%. This suggests that AuthG-Live requires both a sufficient number of channels and optimized microphone placement to effectively detect simulated-wearer attacks. Moreover, for the same number of channels, asymmetric layouts consistently lead to better liveness detection performance. For instance, the 4-channel asymmetric configuration outperforms the 5-channel symmetric layout. This implies that human sound field features are approximately symmetric, and asymmetric microphone layouts can capture richer spatial information. These findings provide practical design guidance for microphone deployment in commercial smart glasses.

Table 14 reports the authentication accuracy for all optimized channel configurations, with and without the bone-conduction (BC) modality. The results show that sound field (SF) features derived from additional air-conducted channels can serve as complementary information to the single AC modality, with a larger number of input channels generally leading to higher authentication accuracy. Compared with SF features, BC features provide a more dominant complementary effect to the AC modality, as the authentication accuracy shows little variation across different SF channel configurations when BC is included, with all achieving around 97%, which is consistently higher than the configurations without BC. These results further suggest that incorporating BC microphones can be more beneficial for authentication performance than relying solely on air-conducted microphones, offering valuable design insights for future smart glasses.

## 5.4 Evaluation with Real-world Products' Configuration

### 5.4.1 Rokid Glass.

Rokid Glass symmetrically embeds four air-conduction microphones on the smart glasses frame, located at the front and middle positions of both the left and right temples, as illustrated in Fig. 11 b. The air-conduction microphones operate at a sampling rate of 16 kHz. To emulate this configuration, we select air-conducted Channels 2, 5, 10, and 13 in our prototype to reconstruct the same spatial layout. Channel 5 is chosen as the reference microphone (the AC modality), and the corresponding AC and SF features are recomputed accordingly. We apply the same data and model modifications described in Sections 5.1 and 5.3. Following the

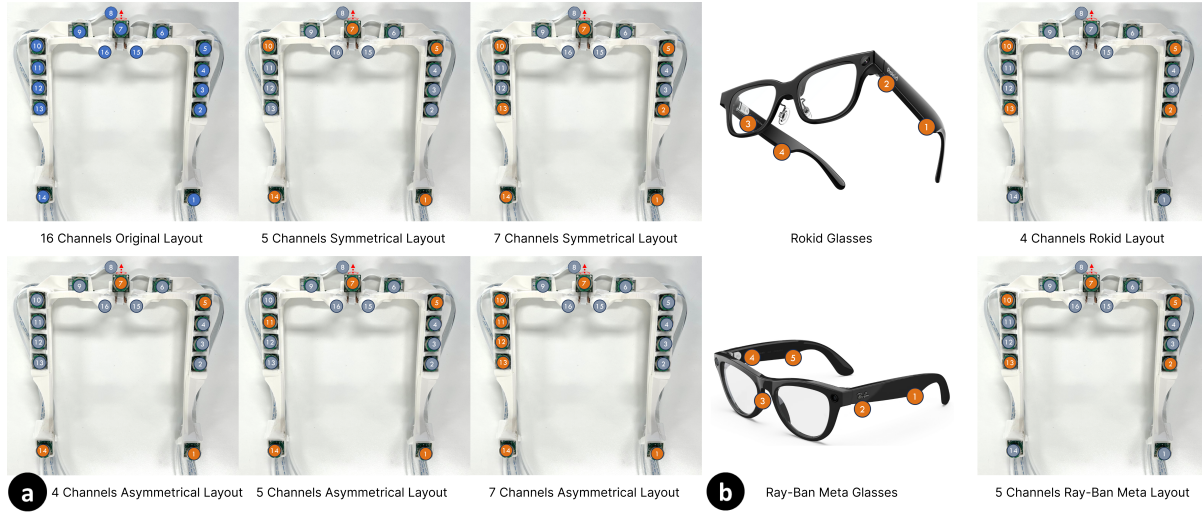


Fig. 11. Liveness detection and authentication accuracy were evaluated under limited input-channel settings. (a) Top row shows the original microphone layout of the prototype and the selected microphones for the 5- and 7-channel symmetric configurations. Bottom row shows the selected microphones for the 4-, 5-, and 7-channel asymmetric configurations. Selected microphones are highlighted in orange. (b) demonstrates the microphone layouts of Rokid Glasses and Ray-Ban Meta Glasses on the left, and the microphones used in our experiments to simulate their recording characteristics on the right, with selected microphones highlighted in orange.

procedures of Benchmark Task 1 and Benchmark Task 3 described in Section 4.2, we evaluate liveness detection and authentication performance.

**5.4.2 Results and Discussion.** Under the Rokid Glass configuration, the liveness detection accuracy (Table 15) for Attack 2 to Attack 6 (more than 96%) remains comparable to that reported in Section 5.3, while Attack 1 and Attack 7 (i.e., attacks from the closest environmental sound sources) cannot be effectively detected, with accuracies of around 50%. This indicates that the symmetric microphone placement in Rokid Glass introduces partial redundancy in capturing symmetric spatial information. Moreover, the relatively compact microphone distribution limits sound field coverage, preventing the system from capturing broader spatial variations. As a result, the liveness detection performance degrades for attacks at closer distances or those produced by simulated wearers.

Table 15. Liveness Detection Accuracy under Real-World Configurations.

Real-World Configurations	Attack 1	Attack 2	Attack 3	Attack 4	Attack 5	Attack 6	Attack 7
Rokid	47.35%	96.33%	96.63%	96.63%	96.63%	95.36%	53.32%
Ray-Ban Meta	49.61%	96.78%	96.78%	96.78%	96.78%	96.78%	96.78%

For authentication (Table 16), AuthG-Net achieves accuracies consistent with the results in Section 5.3, both with (97%) and without (94%) the BC modality. This demonstrates that AuthG-Net is robust to different microphone layouts, even when the AC channel is not placed at the center of the glasses. Considering that the sampling

Table 16. Authentication results under Real-World Configurations.

Real-World Configurations	Rokid		Ray-Ban Meta	
	without BC	with BC	without BC	with BC
Accuracy	94.83%	97.13%	94.86%	97.09%

rate in this setting is 16 kHz, compared with 96 kHz in Section 5.3, we further conclude that AuthG-Net can be deployed on devices with limited sampling rates.

**5.4.3 Ray-Ban Meta.** Ray-Ban Meta integrates five air-conduction microphones, all sampled at 16 kHz as shown in Fig. 11 b. Four of them are placed similarly to those in Rokid Glass, with an additional microphone located at the right nose pad. We reproduced this configuration using Channels 2, 5, 10, 13, and 7, with Channel 7 selected as the AC modality for SF feature extraction. The evaluation procedures and model modifications are the same as those used for the Rokid configuration.

**5.4.4 Results and Discussion.** For the Ray-Ban Meta configuration, the liveness detection accuracy (Table 15) for Attack 2 to Attack 6 reaches similarly high values (above 95%) as those observed for Rokid. The detection accuracy for Attack 7 under the Ray-Ban configuration is also high and comparable to the results reported in Section 5.3, indicating that incorporating more microphones improves detection performance for attacks originating from environmental sound sources. In contrast, Rokid achieves an accuracy of only around 50% for Attack 7. Nevertheless, under our simulated configuration, the detection accuracy for Attack 1 remains around 50%, suggesting that redundancy still exists in capturing symmetric spatial information. Notably, the middle microphone in Ray-Ban Meta is placed on one side of the nose pad, introducing asymmetry in the layout, which can potentially enhance sound field feature capture.

For authentication (Table 16), the simulated Ray-Ban Meta configuration operating at 16 kHz achieves authentication accuracy comparable to that of Rokid and the results reported in Section 5.3. This further strengthens the implication that AuthG-Net can be effectively deployed on devices with limited sampling rates.

## 6 Discussion

In this section, we first summarize the key findings of this work and then highlight the potential applications of the proposed system. Finally, we discuss its limitations and outline possible directions for future research.

### 6.1 Conclusion of Findings

This work proposes the AuthG-Live and AuthG-Net methods and systematically investigates voice liveness detection and authentication on smart glasses through comprehensive multi-acoustic sensing. Based on extensive benchmarking and ablation studies, we summarize the key findings as follows:

- Smart glasses can capture air-conducted (AC), bone-conducted (BC), and sound-field (SF) features that are effective for voice liveness detection and authentication. The spatially distributed microphones on the eyeglass frame naturally capture sound-field characteristics, including inter-channel energy attenuation and propagation delay, while the contact between the nose pads and the user’s face enables the acquisition of bone-conducted vibration signals. Benchmark results in Section 4.5 demonstrate that fusing these modalities leads to high authentication accuracy, indicating that BC and SF features serve as effective complementary information to conventional AC voiceprint features.
- Liveness detection based on sound-field features generalizes better to unseen attacks than attack-driven acoustic methods. Benchmark results in Section 4.5 show that traditional liveness detection approaches

relying on spectral artifacts or attack-specific patterns suffer notable performance degradation when evaluated under unseen attack configurations. In contrast, the proposed AuthG-Live leverages intrinsic physical properties of human speech propagation, enabling robust, attack-device-independent liveness detection without requiring attack samples during training. This indicates that sound-field features cannot be reliably reproduced by replay or simulated-wearer attacks, highlighting the security potential enabled by the smart-glasses form factor.

- Authentication with AuthG-Net demonstrates the effectiveness of multi-acoustic-modal fusion for robust user verification on smart glasses. By jointly modeling AC voiceprint features, BC vibration cues, and SF spatial acoustic characteristics, AuthG-Net consistently outperforms unimodal and bimodal authentication baselines across both standard and cross-utterance authentication tasks. Benchmark results in Section 4.5 show that incorporating BC and SF features significantly improves authentication accuracy and robustness, particularly under conditions where voiceprint-only methods are vulnerable to spoofing or intra-speaker variability. These findings indicate that multi-acoustic fusion is essential for reliable voice authentication on smart glasses.
- AuthG-Live and AuthG-Net maintain strong generalization under practical hardware and deployment constraints. Ablation studies in Section 5 demonstrate that both liveness detection and authentication performance remain competitive even when the number of available microphones or acoustic modalities is reduced to configurations consistent with commercial smart glasses. In particular, sound-field-based liveness detection and multimodal authentication retain high accuracy under limited-channel settings, providing practical design insights for real-world deployment. These results indicate that the proposed methods are not only effective under ideal sensing conditions, but also robust and scalable to realistic smart-glasses hardware configurations.
- AuthGlass establishes the first comprehensive benchmark for voice liveness detection and authentication on smart glasses. By releasing a synchronized, high-sampling-rate, multi-channel dataset along with a unified hardware platform, this work enables fair and systematic comparison across different methods and acoustic modalities. Our findings further reveal that conclusions drawn from conventional single-channel datasets do not directly generalize to smart-glasses-based scenarios. Moreover, through benchmark tasks and ablation studies, we demonstrate the usability and flexibility of the AuthGlass dataset. Owing to its rich input channels, the dataset can be readily partitioned into sub-datasets to support targeted evaluations under specific hardware or modality constraints.

## 6.2 Potential Applications

**6.2.1 AuthG-Live and AuthG-Net.** Our proposed AuthG-Live and AuthG-Net jointly support voice liveness detection and user authentication, thereby enabling secure voice-based interaction on smart glasses. As illustrated in Fig. 1, the system is capable of rejecting various adversarial samples, including attacks initiated by the wearer, attacks from bystanders, and voice commands issued when the device is not being worn. In combination with other on-device sensors, such as a camera, the system can support seamless and secure interaction scenarios. For example, a user may simply look at a payment QR code and issue a voice command such as “Pay the bill” to complete a transaction.

**6.2.2 AuthGlass Dataset.** As demonstrated in Section 4.2, the AuthGlass Dataset is designed to facilitate comprehensive evaluation of voice liveness detection and authentication on smart glasses. By providing synchronized multi-channel audio inputs, the dataset enables systematic ablation studies across different acoustic modalities and input channel configurations, allowing researchers to investigate the contribution of each modality and channel to system performance. Moreover, the dataset includes both genuine samples and attack data collected

from multiple users, which supports rigorous evaluation of authentication and liveness detection under diverse adversarial scenarios.

### 6.3 Limitation and Future Works

*6.3.1 More Configurations of AC Microphones.* Our study demonstrates the effectiveness of AuthG-Live and AuthG-Net incorporating sound field features for liveness detection and authentication. However, we only evaluated a limited set of AC microphone combinations and did not fully optimize the microphone layout. To facilitate future research, we release our dataset to enable further exploration of diverse microphone configurations. Such investigations may provide valuable insights into overall optimal microphone placement and combination strategies, potentially leading to more effective and robust voice authentication systems on smart glasses.

*6.3.2 In the Wild Data and Noise.* Although our AuthGlass dataset consists of many data, it is still recorded in a controlled condition. For practical usage, in-the-wild data need to be recorded and noise should be incorporated for training to enhance the algorithm's robustness. To this end, we open-source our implementation of the smart glasses prototype and the dataset. Future work can replicate the implementation of our prototype and record in-the-wild data, or leverage synthesis method using multi-channel noise dataset [68] for noise incorporation.

*6.3.3 Deployment to Commercial Devices.* As one of the key focuses of this work is the practical applicability of AuthG-Live and AuthG-Net, several challenges remain for deployment on commercial devices. Although the TDT, ERT, and EDF features proposed in this paper have been validated to be effective, their computation still incurs non-negligible processing overhead, which limits the feasibility of real-time authentication. In addition, the system relies on precise synchronization of the microphone arrays to accurately capture sound field information, posing further design and implementation challenges. Furthermore, there is currently no mature solution for embedding bone-conduction microphones into the nose pad of smart glasses, which may restrict signal quality and, consequently, overall system performance. Despite these limitations, ongoing advances in hardware and embedded systems provide promising opportunities to address the computational challenges. While our AuthGlass dataset would pave the way for deployable voice liveness detection and authentication algorithm.

*6.3.4 Sound Field Based Interaction on Smart Glasses.* Our work demonstrates that sound-field features are related to the human speech production process, suggesting potential for broader applications. For example, Proxemic [58] leveraged the time differences between a pair of earbuds to detect mouth-cover gestures. Building on this idea, sound field features could enable hands-on-mouth gesture detection during speech without relying on active acoustic sensing techniques [29].

## 7 Conclusion

This work presents AuthGlass, the first open dataset featuring multi-acoustic-modal, multi-channel recordings for benchmarking voice liveness detection and authentication on smart glasses. Based on AuthGlass, we further propose AuthG-Live for liveness detection and AuthG-Net for voice authentication. Experimental results demonstrate that sound-field and multimodal acoustic features are effective for both liveness detection and authentication, offering practical insights for the design and evaluation of a secure voice-based interaction systems on smart glasses.

## References

- [1] 2025. Eris® E5 Studio Monitor. [https://intl.presonus.com/products/eris-e5-studio-monitor?srsId=AfmBOopFGpJKhO6xHwJ\\_iRWISQZsIOf9Kiw8Wv5WjZ0mKTitWmFcpOnO](https://intl.presonus.com/products/eris-e5-studio-monitor?srsId=AfmBOopFGpJKhO6xHwJ_iRWISQZsIOf9Kiw8Wv5WjZ0mKTitWmFcpOnO).
- [2] 2025. GRAS 45BC KEMAR Head and Torso with Mouth Simulato. <https://www.grasacoustics.com/products/head-torso-simulators-kemar/kemar-non-configured/product/749-45bc>.

- [3] 2025. Infineon IM73D122V01: Ultra-low noise high sensitivity digital XENSIV™ MEMS microphone. <https://www.infineon.com/assets/row/public/documents/24/49/infineon-im73d122-datashet-en.pdf?fileId=8ac78c8c83cd3081018409cafd46db>.
- [4] 2025. Microsoft HoloLens. <https://learn.microsoft.com/en-us/hololens/>.
- [5] 2025. The Munich Automatic Segmentation System MAUS. <https://www.bas.uni-muenchen.de/Bas/BasMAUS.html>.
- [6] 2025. Ray-ban Meta. <https://www.ray-ban.com/usa/ray-ban-meta-ai-glasses>.
- [7] 2025. Rokid Glasses. <https://glasses.rokid.com>.
- [8] 2025. Sonion Voice Picking Unit VPU14aa01. [https://www.ariat-tech.com/parts/VPU14AA01?srsltid=AfmBOoqPZF0ySufKmsHCBWudGqWET3zyMNI78FVCvMtjFjzo8pOYW5\\_n](https://www.ariat-tech.com/parts/VPU14AA01?srsltid=AfmBOoqPZF0ySufKmsHCBWudGqWET3zyMNI78FVCvMtjFjzo8pOYW5_n).
- [9] 2025. Xreal One Pro. <https://www.xreal.com/one-pro>.
- [10] 2026. 16-Element Discrete Microphone Array (Free-Form Layout) Kit. [https://item.taobao.com/item.htm?id=665645262286&mi\\_id=0000\\_37rOJdF150WubGFdgNkOLMtkH1gYxqfX44ihDN0cXo&spm=tbpc.boughtlist.suborder\\_itemtitle.1.24992e8dOxApXT&skuld=4792669972340](https://item.taobao.com/item.htm?id=665645262286&mi_id=0000_37rOJdF150WubGFdgNkOLMtkH1gYxqfX44ihDN0cXo&spm=tbpc.boughtlist.suborder_itemtitle.1.24992e8dOxApXT&skuld=4792669972340).
- [11] Muhammad Ejaz Ahmed, Il-Youp Kwak, Jun Ho Huh, Iljoo Kim, Taekkyung Oh, and Hyounghick Kim. 2020. Void: A fast and light voice liveness detection system. In *29th USENIX Security Symposium (USENIX Security 20)*. 2685–2702.
- [12] Orlando Arias, Jacob Wurm, Khoa Hoang, and Yier Jin. 2015. Privacy and security in internet of things and wearable devices. *IEEE transactions on multi-scale computing systems* 1, 2 (2015), 99–109.
- [13] Pierre Badin and Antoine Serrurier. 2006. Three-dimensional modeling of speech organs: Articulatory data and models. In *Technical Committee of Psychological and Physiological Acoustics*, Vol. 36. The Acoustical Society of Japan, 421–426.
- [14] Logan Blue, Hadi Abdullah, Luis Vargas, and Patrick Traynor. 2018. 2ma: Verifying voice commands via two microphone authentication. In *Proceedings of the 2018 on Asia Conference on Computer and Communications Security*. 89–100.
- [15] Bruno Bouchard, Kevin Bouchard, and Abdenour Bouzouane. 2020. A smart cooking device for assisting cognitively impaired users. *Journal of reliable intelligent environments* 6, 2 (2020), 107–125.
- [16] Pan Chan, Tzipora Halevi, and Nasir Memon. 2015. Glass otp: Secure and convenient user authentication on google glass. In *International Conference on Financial Cryptography and Data Security*. Springer, 298–308.
- [17] Shan Chang, Xinggan Hu, Hongzi Zhu, Wei Liu, and Lei Yang. 2022. Vogue: Secure user voice authentication on wearable devices using gyroscope. In *2022 19th Annual IEEE International Conference on Sensing, Communication, and Networking (SECON)*. IEEE, 361–369.
- [18] Wan-Jung Chang, Liang-Bi Chen, and Yu-Zung Chiou. 2018. Design and implementation of a drowsiness-fatigue-detection system based on wearable smart glasses to increase road safety. *IEEE Transactions on Consumer Electronics* 64, 4 (2018), 461–469.
- [19] Tao Chen, Yongjie Yang, Chonghao Qiu, Xiaoran Fan, Xiuzhen Guo, and Longfei Shangguan. 2024. Enabling hands-free voice assistant activation on earphones. In *Proceedings of the 22nd Annual International Conference on Mobile Systems, Applications and Services*. 155–168.
- [20] Ryan M. Corey, Matthew D. Skarha, and Andrew C. Singer. 2019. Massive Distributed Microphone Array Dataset. doi:10.13012/B2IDB-6216881\_V1
- [21] Phillip L. De Leon, Michael Pucher, Junichi Yamagishi, Inma Hernaez, and Ibon Saratxaga. 2012. Evaluation of Speaker Verification Security and Detection of HMM-Based Synthetic Speech. *IEEE Transactions on Audio, Speech, and Language Processing* 20, 8 (2012), 2280–2290. doi:10.1109/TASL.2012.2201472
- [22] Yuemeng Du, Jingyan Qin, Shujing Zhang, Sha Cao, and Jinhua Dou. 2018. Voice user interface interaction design research based on user mental model in autonomous vehicle. In *International Conference on Human-Computer Interaction*. Springer, 117–132.
- [23] Serife Kucur Ergünay, Elie Khoury, Alexandros Lazaridis, and Sébastien Marcel. 2015. On the vulnerability of speaker verification to realistic voice spoofing. In *2015 IEEE 7th international conference on biometrics theory, applications and systems (BTAS)*. IEEE, 1–6.
- [24] Huan Feng, Kassem Fawaz, and Kang G Shin. 2017. Continuous authentication for voice assistants. In *Proceedings of the 23rd Annual International Conference on Mobile Computing and Networking*. 343–355.
- [25] Eira Friström, Elias Lius, Niki Ulmanen, Paavo Hietala, Pauliina Kärkkäinen, Tommi Mäkinen, Stephan Sigg, and Rainhard Dieter Findling. 2019. Free-form gaze passwords from cameras embedded in smart glasses. In *Proceedings of the 17th International Conference on Advances in Mobile Computing & Multimedia*. 136–144.
- [26] Bhanuka Gamage. 2024. AI-Enabled Smart Glasses for People with Severe Vision Impairments. *ACM SIGACCESS Accessibility and Computing* 137 (2024), 1–1.
- [27] Yaroslav Ganin and Victor Lempitsky. 2015. Unsupervised domain adaptation by backpropagation. In *International conference on machine learning*. PMLR, 1180–1189.
- [28] Yang Gao, Yincheng Jin, Jagmohan Chauhan, Seokmin Choi, Jiyang Li, and Zhanpeng Jin. 2021. Voice in ear: Spoofing-resistant and passphrase-independent body sound authentication. *Proceedings of the ACM on Interactive, Mobile, Wearable and Ubiquitous Technologies* 5, 1 (2021), 1–25.
- [29] Kaiyi Guo, Tianyu Wu, Yang Gao, Qian Zhang, and Dong Wang. 2025. EchoTouch: Low-power Face-touching Behavior Recognition Using Active Acoustic Sensing on Glasses. *Proc. ACM Interact. Mob. Wearable Ubiquitous Technol.* 9, 2, Article 31 (June 2025), 33 pages. doi:10.1145/3729481

- [30] Jibo He, Jake Ellis, William Choi, and Pingfeng Wang. 2015. Driving While Reading Using Google Glass Versus Using a Smartphone: Which is More Distracting to Driving Performance?. In *Driving Assessment Conference*, Vol. 8. University of Iowa.
- [31] Ruiwen He, Yushi Cheng, Zhicong Zheng, Xiaoyu Ji, and Wenyuan Xu. 2024. Fast and lightweight voice replay attack detection via time-frequency spectrum difference. *IEEE Internet of Things Journal* 11, 18 (2024), 29798–29810.
- [32] Chenpei Huang, Hui Zhong, Pavana Prakash, Dian Shi, Xu Yuan, and Miao Pan. 2025. Eve said yes: Airbone authentication for head-wearable smart voice assistant. *IEEE Transactions on Mobile Computing* (2025).
- [33] Yuliy Iliev and Galina Ilieva. 2022. A framework for smart home system with voice control using NLP methods. *Electronics* 12, 1 (2022), 116.
- [34] MD Rasel Islam, Doyoung Lee, Liza Suraiya Jahan, and Ian Oakley. 2018. Glasspass: Tapping gestures to unlock smart glasses. In *Proceedings of the 9th Augmented Human International Conference*. 1–8.
- [35] Jingun Jung, Sangyoon Lee, Jiwoo Hong, Eunhye Youn, and Geehyuk Lee. 2020. Voice+ tactile: Augmenting in-vehicle voice user interface with tactile touchpad interaction. In *Proceedings of the 2020 CHI Conference on Human Factors in Computing Systems*. 1–12.
- [36] Madhu R Kamble, Hardik B Sailor, Hemant A Patil, and Haizhou Li. 2020. Advances in anti-spoofing: from the perspective of ASVspoof challenges. *APSIPA Transactions on Signal and Information Processing* 9 (2020), e2.
- [37] Navdeep Kaur and Parminder Singh. 2023. Conventional and contemporary approaches used in text to speech synthesis: A review. *Artificial Intelligence Review* 56, 7 (2023), 5837–5880.
- [38] Lawrence George Kersta. 1962. Voiceprint identification. *The Journal of the Acoustical Society of America* 34, 5\_Supplement (1962), 725–725.
- [39] Smita Khade, Swati Ahirrao, Shraddha Phansalkar, Ketan Kotecha, Shilpa Gite, and Sudeep D Thepade. 2021. Iris liveness detection for biometric authentication: A systematic literature review and future directions. *Inventions* 6, 4 (2021), 65.
- [40] Sunwook Kim, Maury A Nussbaum, and Joseph L Gabbard. 2016. Augmented reality “smart glasses” in the workplace: industry perspectives and challenges for worker safety and health. *IIE transactions on occupational ergonomics and human factors* 4, 4 (2016), 253–258.
- [41] Tomi Kinnunen, Md Sahidullah, Mauro Falcone, Luca Costantini, Rosa González Hautamäki, Dennis Thomsen, Achintya Sarkar, Zheng-Hua Tan, Héctor Delgado, Massimiliano Todisco, et al. 2017. Reddotts replayed: A new replay spoofing attack corpus for text-dependent speaker verification research. In *2017 IEEE International conference on acoustics, speech and signal processing (ICASSP)*. IEEE, 5395–5399.
- [42] Huining Li, Chenhan Xu, Aditya Singh Rathore, Zhengxiong Li, Hanbin Zhang, Chen Song, Kun Wang, Lu Su, Feng Lin, Kui Ren, et al. 2020. VocalPrint: Exploring a resilient and secure voice authentication via mmWave biometric interrogation. In *Proceedings of the 18th Conference on Embedded Networked Sensor Systems*. 312–325.
- [43] Jingjin Li, Chao Chen, Mostafa Rahimi Azghadi, Hossein Ghodosi, Lei Pan, and Jun Zhang. 2023. Security and privacy problems in voice assistant applications: A survey. *Computers & Security* 134 (2023), 103448.
- [44] Ke Li, Devansh Agarwal, Ruidong Zhang, Vipin Gunda, Tianjun Mo, Saif Mahmud, Boao Chen, François Guimbretiére, and Cheng Zhang. 2024. SonicID: User Identification on Smart Glasses with Acoustic Sensing. *Proceedings of the ACM on Interactive, Mobile, Wearable and Ubiquitous Technologies* 8, 4 (2024), 1–27.
- [45] Yue Li, Xueru Gao, Qipeng Song, Yao Wang, Pin Lyu, and Haibin Zhang. 2024. BoneAuth: A Bone Conduction-Based Voice Liveness Authentication for Voice Assistants. *IEEE Internet of Things Journal* (2024).
- [46] Yung-Hui Li and Po-Jen Huang. 2017. An accurate and efficient user authentication mechanism on smart glasses based on iris recognition. *Mobile Information Systems* 2017, 1 (2017), 1281020.
- [47] Zhuohang Li, Cong Shi, Tianfang Zhang, Yi Xie, Jian Liu, Bo Yuan, and Yingying Chen. 2021. Robust detection of machine-induced audio attacks in intelligent audio systems with microphone array. In *Proceedings of the 2021 ACM SIGSAC Conference on Computer and Communications Security*. 1884–1899.
- [48] Li Lu, Jiadi Yu, Yingying Chen, and Yan Wang. 2020. Vocallock: Sensing vocal tract for passphrase-independent user authentication leveraging acoustic signals on smartphones. *Proceedings of the ACM on Interactive, Mobile, Wearable and Ubiquitous Technologies* 4, 2 (2020), 1–24.
- [49] Isaias Majil, Mau-Tsuen Yang, and Sophia Yang. 2022. Augmented reality based interactive cooking guide. *Sensors* 22, 21 (2022), 8290.
- [50] Mitchell McLaren, Luciana Ferrer, Diego Castan, and Aaron Lawson. 2016. The speakers in the wild (SITW) speaker recognition database.. In *Interspeech*. 818–822.
- [51] Yan Meng, Jiachun Li, Matthew Pillari, Arjun Deopujari, Liam Brennan, Hafsa Shamsie, Haojin Zhu, and Yuan Tian. 2022. Your microphone array retains your identity: A robust voice liveness detection system for smart speakers. In *31st USENIX Security Symposium (USENIX Security 22)*. 1077–1094.
- [52] Arsha Nagrani, Joon Son Chung, and Andrew Senior. 2017. Voxceleb: a large-scale speaker identification dataset. *arXiv preprint arXiv:1706.08612* (2017).
- [53] AN Nithyaa, R Premkumar, N Sudhandirapriya, and R Durga. 2023. Eye Glasses for the Visually Challenged Using Artificial Intelligence Application. In *International Conference on Soft Computing and Signal Processing*. Springer, 347–360.

- [54] Francesca Palermo, Luca Casciano, Lokmane Demagh, Aurelio Teliti, Niccolò Antonello, Giacomo Gervasoni, Hazem Hesham Yousef Shalby, Marco Brando Paracchini, Simone Mentasti, Hao Quan, et al. 2025. Advancements in Context Recognition for Edge Devices and Smart Eyewear: Sensors and Applications. *IEEE Access* (2025).
- [55] Seung-A Park, Sun-Beom Kwon, Yong Woo Lee, Jejin Jo, Jun-Seob Kim, Mee Lan Han, and Dooho Choi. 2025. Toward almost-zero fault acceptance of deep learning-based voice authentication using small training dataset. *Soft Computing* (2025), 1–12.
- [56] Ge Peng, Gang Zhou, David T Nguyen, Xin Qi, Qing Yang, and Shuangquan Wang. 2016. Continuous authentication with touch behavioral biometrics and voice on wearable glasses. *IEEE transactions on human-machine systems* 47, 3 (2016), 404–416.
- [57] Lam Pham, Phat Lam, Dat Tran, Hieu Tang, Tin Nguyen, Alexander Schindler, Florian Skopik, Alexander Polonsky, and Hai Canh Vu. 2025. A comprehensive survey with critical analysis for deepfake speech detection. *Computer Science Review* 57 (2025), 100757.
- [58] Yue Qin, Chun Yu, Zhaoheng Li, Mingyuan Zhong, Yukang Yan, and Yuanchun Shi. 2021. Proximic: Convenient voice activation via close-to-mic speech detected by a single microphone. In *Proceedings of the 2021 CHI Conference on Human Factors in Computing Systems*. 1–12.
- [59] P Selvi Rajendran, Padmaveni Krishnan, and D John Aravindhar. 2020. Design and implementation of voice assisted smart glasses for visually impaired people using google vision api. In *2020 4th International Conference on Electronics, Communication and Aerospace Technology (ICECA)*. IEEE, 1221–1224.
- [60] P. Selvi Rajendran, Padmaveni Krishnan, and D. John Aravindhar. 2020. Design and Implementation of Voice Assisted Smart Glasses for Visually Impaired People Using Google Vision API. In *2020 4th International Conference on Electronics, Communication and Aerospace Technology (ICECA)*. 1221–1224. doi:10.1109/ICECA49313.2020.9297553
- [61] Suranga Seneviratne, Yining Hu, Tham Nguyen, Guohao Lan, Sara Khalifa, Kanchana Thilakarathna, Mahbub Hassan, and Aruna Seneviratne. 2017. A survey of wearable devices and challenges. *IEEE Communications Surveys & Tutorials* 19, 4 (2017), 2573–2620.
- [62] Cong Shi, Yan Wang, Yingying Chen, Nitesh Saxena, and Chen Wang. 2020. Wearid: Low-effort wearable-assisted authentication of voice commands via cross-domain comparison without training. In *Proceedings of the 36th Annual Computer Security Applications Conference*. 829–842.
- [63] Ryohei Shioji, Shin-ichi Ito, Momoyo Ito, and Minoru Fukumi. 2018. Personal authentication and hand motion recognition based on wrist EMG analysis by a convolutional neural network. In *2018 IEEE International Conference on Internet of Things and Intelligence System (IOTAIS)*. IEEE, 184–188.
- [64] Sayaka Shiota, Fernando Villavicencio, Junichi Yamagishi, Nobutaka Ono, Isao Echizen, and Tomoko Matsui. 2015. Voice liveness detection algorithms based on pop noise caused by human breath for automatic speaker verification. In *INTERSPEECH 2015 16th Annual Conference of the International Speech Communication Association*. International Speech Communication Association, France, 239–243.
- [65] Yao Song, Yanpu Yang, and Peiyao Cheng. 2022. The investigation of adoption of voice-user interface (VUI) in smart home systems among Chinese older adults. *Sensors* 22, 4 (2022), 1614.
- [66] Yu Su, Yongjiao Li, and Zhu Cao. 2023. Gait-based privacy protection for smart wearable devices. *IEEE Internet of Things Journal* 11, 2 (2023), 3497–3509.
- [67] Ashique T P, Hridya Girish, Ivine P Sabu, Thomas Raju, and Anoop V. 2025. AI-Powered Smart Glasses for Real-Time Speech-to-Text Transcription. In *2025 4th International Conference on Advances in Computing, Communication, Embedded and Secure Systems (ACCESS)*. 442–445. doi:10.1109/ACCESS65134.2025.11135871
- [68] Joachim Thiemann, Nobutaka Ito, and Emmanuel Vincent. 2013. DEMAND: a collection of multi-channel recordings of acoustic noise in diverse environments. (*No Title*) (2013).
- [69] Mohamed A Torad, Belgacem Bouallegue, and Abdelmoty M Ahmed. 2022. A voice controlled smart home automation system using artificial intelligent and internet of things. *TELKOMNIKA (Telecommunication Computing Electronics and Control)* 20, 4 (2022), 808–816.
- [70] Andreas Triantafyllopoulos, Björn W Schuller, Gökçe İymen, Metin Sezgin, Xiangheng He, Zijiang Yang, Panagiotis Tzirakis, Shuo Liu, Silvan Mertens, Elisabeth André, et al. 2023. An overview of affective speech synthesis and conversion in the deep learning era. *Proc. IEEE* 111, 10 (2023), 1355–1381.
- [71] Eric Tzeng, Judy Hoffman, Kate Saenko, and Trevor Darrell. 2017. Adversarial discriminative domain adaptation. In *Proceedings of the IEEE conference on computer vision and pattern recognition*. 7167–7176.
- [72] Suresh Veesa and Madhusudan Singh. 2025. Deep learning countermeasures for detecting replay speech attacks: a review. *International Journal of Speech Technology* 28, 1 (2025), 39–51.
- [73] Qian Wang, Xiu Lin, Man Zhou, Yanjiao Chen, Cong Wang, Qi Li, and Xiangyang Luo. 2019. VoicePop: A Pop Noise based Anti-spoofing System for Voice Authentication on Smartphones. In *IEEE INFOCOM 2019 - IEEE Conference on Computer Communications*. 2062–2070. doi:10.1109/INFOCOM.2019.8737422
- [74] Yao Wang, Wandong Cai, Tao Gu, Wei Shao, Yannan Li, and Yong Yu. 2019. Secure your voice: An oral airflow-based continuous liveness detection for voice assistants. *Proceedings of the ACM on interactive, mobile, wearable and ubiquitous technologies* 3, 4 (2019), 1–28.
- [75] Emily Wenger, Max Bronckers, Christian Cianfarani, Jenna Cryan, Angela Sha, Haitao Zheng, and Ben Y Zhao. 2021. "Hello, It's Me": Deep Learning-based Speech Synthesis Attacks in the Real World. In *Proceedings of the 2021 ACM SIGSAC Conference on Computer and Communications Security*. 235–251.

Table 17. Passphrase Set Used in the Experiments

(1) Hi siri	(2) Hi google	(3) Hi alexa
(4) Pay the bill	(5) Call tom	(6) Turn on bluetooth
(7) Take a photo	(8) Play some music	(9) Show me my first message
(10) Send an email to john	(11) Check my voicemail	(12) What's my appointment
(13) Set an alarm	(14) Thank you	(15) A hundred dollars

- [76] Junichi Yamagishi, Xin Wang, Massimiliano Todisco, Md Sahidullah, Jose Patino, Andreas Nautsch, Xuechen Liu, Kong Aik Lee, Tomi Kinnunen, Nicholas Evans, et al. 2021. ASVspoof 2021: accelerating progress in spoofed and deepfake speech detection. *arXiv preprint arXiv:2109.00537* (2021).
- [77] Chen Yan, Xiaoyu Ji, Kai Wang, Qinrong Jiang, Zizhi Jin, and Wenyuan Xu. 2022. A survey on voice assistant security: Attacks and countermeasures. *Comput. Surveys* 55, 4 (2022), 1–36.
- [78] Chen Yan, Yan Long, Xiaoyu Ji, and Wenyuan Xu. 2019. The catcher in the field: A fieldprint based spoofing detection for text-independent speaker verification. In *Proceedings of the 2019 ACM SIGSAC Conference on Computer and Communications Security*. 1215–1229.
- [79] Bing Yang, Changsheng Quan, Yabo Wang, Pengyu Wang, Yujie Yang, Ying Fang, Nian Shao, Hui Bu, Xin Xu, and Xiaofei Li. 2024. RealMAN: A real-recorded and annotated microphone array dataset for dynamic speech enhancement and localization. *Advances in Neural Information Processing Systems* 37 (2024), 105997–106019.
- [80] Junshuang Yang, Yanyan Li, and Mengjun Xie. 2015. Motionauth: Motion-based authentication for wrist worn smart devices. In *2015 IEEE International conference on pervasive computing and communication workshops (PerCom Workshops)*. IEEE, 550–555.
- [81] Qiang Yang, Kaiyan Cui, and Yuanqing Zheng. 2023. VoShield: Voice liveness detection with sound field dynamics. In *IEEE INFOCOM 2023-IEEE Conference on Computer Communications*. IEEE, 1–10.
- [82] Jiangyan Yi, Chenglong Wang, Jianhua Tao, Xiaohui Zhang, Chu Yuan Zhang, and Yan Zhao. 2023. Audio deepfake detection: A survey. *arXiv preprint arXiv:2308.14970* (2023).
- [83] Linghan Zhang, Sheng Tan, Yingying Chen, and Jie Yang. 2022. A continuous articulatory-gesture-based liveness detection for voice authentication on smart devices. *IEEE Internet of Things Journal* 9, 23 (2022), 23320–23331.
- [84] Linghan Zhang, Sheng Tan, Jie Yang, and Yingying Chen. 2016. Voicelive: A phoneme localization based liveness detection for voice authentication on smartphones. In *Proceedings of the 2016 ACM SIGSAC Conference on Computer and Communications Security*. 1080–1091.
- [85] Tianfang Zhang, Qiufan Ji, Zhengkun Ye, Md Mojibur Rahman Redoy Akanda, Ahmed Tanvir Mahdad, Cong Shi, Yan Wang, Nitesh Saxena, and Yingying Chen. 2024. SAFARI: Speech-Associated Facial Authentication for AR/VR Settings via Robust Vibration Signatures. In *Proceedings of the 2024 ACM SIGSAC Conference on Computer and Communications Security*. 153–167.
- [86] Zhan Zhang, Enze Bai, Aram Stepanian, Swathi Jagannath, and Sun Young Park. 2025. Touchless interaction for smart glasses in emergency medical services: user needs and experiences. *International Journal of Human-Computer Interaction* 41, 5 (2025), 2984–3003.
- [87] Tianming Zhao, Yan Wang, Jian Liu, Yingying Chen, Jerry Cheng, and Jiadi Yu. 2020. Trueheart: Continuous authentication on wrist-worn wearables using ppg-based biometrics. In *IEEE INFOCOM 2020-IEEE Conference on Computer Communications*. IEEE, 30–39.
- [88] Chu-Xiao Zuo, Zhi-Jun Jia, and Wu-Jun Li. 2024. AdvTTS: Adversarial Text-to-Speech Synthesis Attack on Speaker Identification Systems. In *ICASSP 2024-2024 IEEE International Conference on Acoustics, Speech and Signal Processing (ICASSP)*. IEEE, 4840–4844.

## A Appendix

### A.1 Passphrase Set and Rationale

Table 17 lists the 15 passphrases used in our experiments. Each phrase contains no more than five words, enabling the evaluation of liveness detection and speaker authentication. They were selected from common daily expressions that could serve as practical voice commands, ensuring the scenarios are realistic for everyday use. In addition, the set was chosen to collectively cover most English vowels and consonants, providing representative phonetic content so that the model's performance is not biased by the specific phonemes of individual phrases.

### A.2 Performance of the Original Implementation of Liveness Detection Methods

In Section 4.5, we evaluated the accuracy of previous methods on multi-channel microphone data in Benchmark Task 1. In some of the original papers, only a small number of microphones were used. Based on the descriptions

in the original works, we also implemented the original versions of the selected methods. The liveness detection accuracy results are presented in Table 18.

Table 18. Comparison on Liveness Detection Accuracy Using the Original Versions of the Selected Methods.

<b>Attacked by</b>	<b>Attack 1</b>	<b>Attack 2</b>	<b>Attack 3</b>	<b>Attack 4</b>	<b>Attack 5</b>	<b>Attack 6</b>	<b>Attack 7</b>
VOID	99.43%	99.14%	99.21%	98.81%	98.69%	98.56%	96.60%
Fast and Lightweight	99.92%	99.95%	99.97%	100.00%	99.99%	99.64%	99.29%
Boneauth	91.80%	84.42%	69.70%	85.62%	75.41%	78.11%	68.44%
Eve Said Yes	20.95%	53.15%	85.58%	64.60%	55.13%	37.01%	24.21%
Cafield	78.69%	100.00%	100.00%	100.00%	99.96%	100.00%	100.00%
Voshield	100.00%	100.00%	100.00%	100.00%	100.00%	100.00%	100.00%

Received 20 February 2007; revised 12 March 2009; accepted 5 June 2009